INFORMATION TO USERS

This manuscript has been reproduced from the microfilm master. UMI films the text directly from the original or copy submitted. Thus, some thesis and dissertation copies are in typewriter face, while others may be from any type of computer printer.

The quality of this reproduction is dependent upon the quality of the copy submitted. Broken or indistinct print, colored or poor quality illustrations and photographs, print bleedthrough, substandard margins, and improper alignment can adversely affect reproduction.

In the unlikely event that the author did not send UMI a complete manuscript and there are missing pages, these will be noted. Also, if unauthorized copyright material had to be removed, a note will indicate the deletion.

Oversize materials (e.g., maps, drawings, charts) are reproduced by sectioning the original, beginning at the upper left-hand corner and continuing from left to right in equal sections with small overlaps.

ProQuest Information and Learning
300 North Zeeb Road, Ann Arbor, MI 48106-1346 USA
800-521-0600

University of Alberta

Multiple Model Robust Control of a Boiler System

by

Rong Zhou 

A thesis submitted to the Faculty of Graduate Studies and Research in partial fulfillment of the requirements for the degree of Master of Science

Department of Electrical & Computer Engineering

Edmonton, Alberta
Spring 2005

Abstract

This thesis is concerned with control design for cogeneration systems. Cogeneration systems are large industrial plants characterized by being high order, complex nonlinear plants. Given their complexity, nonlinear control techniques are usually impossible to use. Linear control techniques, on the other hand, overlook the nonlinear nature of the plant and this fail to achieve good performance throughout an entire operating region.

In this thesis we investigate a multiple model approach to the control of cogeneration systems. We controlled boiler system that is part of the Syncrude Canada Ltd integrated energy facility.

Three local linear models around different operating points are identified first. Then companion H_∞ controllers are designed, and a controller switching algorithm is presented. All the controllers, observers and switching algorithm are realized and connected with the SYNSIM simulation package. The simulation results show that our multiple robust controller reach good performance across the entire nonlinear operating space.

Acknowledgement

I wish to thank Dr. H.J. Marquez most sincerely for his invaluable direction and encouragement during the period of study and research. Without his helpful and knowledgeable advice, I would have never finished this thesis.

Table of Contents

List of Tables

List of Figures

Chapter 1

Introduction

1.1 Background

This thesis considers control systems design for cogeneration systems. These plants are large, interconnected nonlinear systems and present a challenge to control engineers. The Syncrude Canada Ltd. (SCL) integrated energy facility is one such a plant. The plant utilizes a complex header system for steam distribution, which includes headers at four different pressure levels (6.306, 4.24, 1.068 and 0.372 MPa). The 6.306MPa header receives steam from three utility type boilers. These three utility boilers are used to regulate the steam pressure, and thus, these boilers play an important role in the overall plant operation. The utility boilers in the plant exhibits complex nonlinearity, and controlling their operation presents a challenge to control systems engineers. At present, multiloop (decentralized) proportional plus integral (PI) type controllers are employed to control the boilers [18].

Although these controllers, for the most part, work well, large oscillatory behavior has been observed in the certain load conditions. The reason, can be attributed to the nonlinear characteristics of the plant along with the linear PI controllers that can only capture the "local" behavior of the plant.

Currently there are a variety of nonlinear controller design methods. Gain schedul-

ing is an effective method for nonlinear control design in practice[1]. In section 1.2 this method is reviewed. It is impossible to obtain an accurate model for the boiler system. Robust control design is an effective approach for the inaccurate model. In section 1.3 the robust control is briefly reviewed.

1.2 Gain scheduling

Gain scheduling is one method to deal with controller design for a nonlinear plant. Various design techniques can be viewed as gain scheduling. For example, controller gain values are adjusted according to operating conditions; an appropriate controller is chosen among several controllers according to certain conditions; blending multiple controller output to form a final controller output.

The features of gain scheduling are listed below[1]:

- Powerful linear controller design tools are employed to solve difficult nonlinear problems.
- There is no strict requirement on the plant model.
- Gain scheduling is used to decompose the complex nonlinear control problem into several simpler sub-problems.
- When operating area is changed a gain scheduling controller is able to respond quickly.
- Compared with other nonlinear controller design approaches the computation burden of gain scheduling is much lower.
- Gain scheduling always includes several ad hoc steps.

Since 1990 gain scheduling had attracted interest of more and more researchers [1]. There is an overwhelming number of papers involving innovative gain scheduling

approaches. Generally, all the gain scheduling approaches can be set into two categories. One is gain scheduling in the sense of continuously varying the controller coefficients, and the other is controller switching or blending. The following section will provide an overview for the two categories.

1.2.1 Gain scheduling of continuously varying the controller coefficients

Gain scheduling in the sense of continuously varying the controller coefficients means that the designed controller coefficients vary according to the value of scheduling variables. Generally, there exists four-step controller design procedure for gain scheduling of continuously varying the controller coefficients. Researchers present a quantity of different techniques for each design step.

The first design step is to obtain a linear parameter-varying model for the plant. There exists two main approaches to compute a linear parameter-varying model. The most common approach is linearization scheduling method which is to realize the linearization of the nonlinear plant around a family of equilibrium points, and the common used linearization techniques is Jacobian linearization. By using Jacobian linearization a parametrized family of linearized plants is obtained. Moreover, the parametrization relates to values of the scheduling variables. Another approach to obtain a linear parameter-varying model is quasi-LPV (Linear Parameter-Varying) method. In quasi-LPV method the plant nonlinear models is rewritten so that the nonlinearities are hidden as time-varying parameters, and this time-varying parameters is used as scheduling variables.

The second design step is to design linear controllers using the sound linear controller design theory for the linear parameter-varying plant model that is obtained from the first design step.

The third design step is to vary the controller coefficients according to the current value of the scheduling variables. This step result in the name of gain scheduling.

According to LPV modeling techniques there exists various gain scheduling implementation methods.

The last design step is performance assessment. In this step the local stability issue and the performance properties of the gain scheduled controller are analyzed.

Using different methods in each design step creates various gain scheduling controller design methods. Typical techniques are reviewed in the following part.

1.2.1.1 Linear parameter-varying (LPV) model

Consider the following nonlinear plant

$$\begin{aligned} \dot{x} &= a(x,u,w,v) \\ z &= c_1(x,u,w,v) \\ y &= c_2(x,w,v) \end{aligned} \tag{1.1}$$

where,

x is the state, u is the input, z is an error signal to be controlled, y is output variable, w denotes exogenous inputs which capture parametric dependence of the plant on exogenous variables, v denotes external "input functions" such as reference commands, disturbances and noises.

As discussed in Section 1.2.1 there are two approaches to obtain a linear parameter-varying model: one is the classical Jacobian linearization approach and the other is the quasi-LPV approach.

Jacobian linearization approach

Jacobian linearization approach is a linearization method around some plant equilibrium points. Here x_e, u_e, w_e, and v_e is an equilibrium point of nonlinear plant (1.1), i.e. $a(x_e,u_e,w_e,v_e) = 0$. A set of equilibrium points parametrized by a scheduling

variable σ is described in the following definition [1].

Definition 1 *The functions $x_e(\sigma), u_e(\sigma), w_e(\sigma)$ and $v_e(\sigma)$ define an equilibrium family for the plant (1.1) on the set S if $a(x_e(\sigma), u_e(\sigma), w_e(\sigma), v_e(\sigma)) = 0$, $\sigma \in S$.*

Correspondingly, the error equilibrium family is,

$$z_e(\sigma) = c_1(x_e(\sigma), u_e(\sigma), w_e(\sigma), v_e(\sigma)), \sigma \in S$$

and the measured output equilibrium family is,

$$y_e(\sigma) = c_2(x_e(\sigma), w_e(\sigma), v_e(\sigma)), \sigma \in S$$

Normally the scheduling variable σ depends on the exogenous input w and y. Thus, the scheduling variable σ becomes a time-varying input signal to the gain scheduled controller implementation. Obviously, the linearization model of nonlinear plant (1.1) can be represented as follows,

$$\begin{bmatrix} \dot{x}_\delta \\ z_\delta \\ y_\delta \end{bmatrix} = \begin{bmatrix} A(\sigma) & B_1(\sigma) & B_2(\sigma) \\ C_1(\sigma) & D_{11}(\sigma) & D_{12}(\sigma) \\ C_2(\sigma) & D_{21}(\sigma) & 0 \end{bmatrix} \begin{bmatrix} x_\delta \\ v_\delta \\ u_\delta \end{bmatrix}, \sigma \in S, \tag{1.2}$$

where,

$$
\begin{aligned}
A(\sigma) &= \frac{\partial a}{\partial x}(x_e(\sigma), u_e(\sigma), w_e(\sigma), v_e(\sigma)), \\
B_1(\sigma) &= \frac{\partial a}{\partial v}(x_e(\sigma), u_e(\sigma), w_e(\sigma), v_e(\sigma)), \\
B_2(\sigma) &= \frac{\partial a}{\partial u}(x_e(\sigma), u_e(\sigma), w_e(\sigma), v_e(\sigma)), \\
C_1(\sigma) &= \frac{\partial c_1}{\partial x}(x_e(\sigma), u_e(\sigma), w_e(\sigma), v_e(\sigma)), \\
D_{11}(\sigma) &= \frac{\partial c_1}{\partial v}(x_e(\sigma), u_e(\sigma), w_e(\sigma), v_e(\sigma)), \\
D_{12}(\sigma) &= \frac{\partial c_1}{\partial u}(x_e(\sigma), u_e(\sigma), w_e(\sigma), v_e(\sigma)), \\
C_2(\sigma) &= \frac{\partial y}{\partial x}(x_e(\sigma), u_e(\sigma), w_e(\sigma), v_e(\sigma)), \\
D_{21}(\sigma) &= \frac{\partial y}{\partial v}(x_e(\sigma), u_e(\sigma), w_e(\sigma), v_e(\sigma)),
\end{aligned} \tag{1.3}
$$

and all the variables are deviation variables, i.e.

$$
\begin{aligned}
x_\delta(t) &= x(t) - x_e(\sigma) \\
z_\delta(t) &= z(t) - z_e(\sigma) \\
y_\delta(t) &= y(t) - y_e(\sigma) \\
v_\delta(t) &= v(t) - v_e(\sigma) \\
u_\delta(t) &= u(t) - u_e(\sigma)
\end{aligned} \tag{1.4}
$$

According to Equation (1.2) there exists a local linearization model for the nonlinear plant at each fixed σ about the corresponding equilibrium. Obviously, Equation (1.2) represents a linear parameter-varying model.

Quasi-LPV model

The idea of quasi-LPV model description approach is to rewrite the nonlinear plant so that the nonlinear terms can be hidden with newly defined, time-varying parameters that then included in the scheduling variable, in addition to w.

The state of plant (1.1) is assumed can be divided into two partitions:

$$x(t) = \begin{bmatrix} x_a(t) \\ x_b(t) \end{bmatrix} \tag{1.5}$$

where,

x_a denotes the part of the states that are rewritten as parameters with,

$$\sigma(t) = \begin{bmatrix} x_a(t) \\ w(t) \end{bmatrix} \tag{1.6}$$

x_b denotes the remaining states.

And the nonlinear plant (1.1) is assumed can be written in the quasi-LPV form,

$$\begin{bmatrix} \dot{x}_a \\ \dot{x}_b \\ z \\ y \end{bmatrix} = \begin{bmatrix} A_{11}(\sigma) & A_{12}(\sigma) & B_{1a}(\sigma) & B_{2a}(\sigma) \\ A_{21}(\sigma) & A_{22}(\sigma) & B_{1b}(\sigma) & B_{2b}(\sigma) \\ C_{1a}(\sigma) & C_{1b}(\sigma) & D_{11}(\sigma) & D_{12}(\sigma) \\ C_{2a}(\sigma) & C_{2b}(\sigma) & D_{21}(\sigma) & D_{22}(\sigma) \end{bmatrix} \begin{bmatrix} x_a \\ x_b \\ v \\ \hat{u}(\sigma, u) \end{bmatrix} \tag{1.7}$$

where,

$\sigma(t)$ is scheduling variable which is a time-varying parameter.

$\hat{u}(\sigma, u)$ is assumed to be invertible with respect to u, i.e. following equality is satisfied,

$$\hat{u}^{-1}(\sigma, \hat{u}(\sigma, u)) = u \tag{1.8}$$

If the nonlinear plant (1.1) can be rewritten into the form as (1.7) then a linear controller can be obtained by (1.8).

1.2.1.2 Linear gain scheduling controller design

As discussed in Section 1.2.1 the second design step is to design linear controllers for the linear parameter varying model and the third step is to vary the coefficients of the linear controller. Several methods are presented to design linear gain scheduling controller. In summary there are two main controller design methods. One method is point designs. i.e. A family of linear controllers are designed corresponding to selected equilibria. Then a final controller output is obtained by using different techniques. The other method is directly design controller via some particular methods. e.g. LPV or LFT method.

Point designs

Since model (1.2) is a model family parametrized by σ the corresponding controller family is also parametrized by σ. The controller family can be described as follows,

$$\begin{bmatrix} \dot{x}_\delta^c \\ u_\delta \end{bmatrix} = \begin{bmatrix} F(\sigma) & G(\sigma) \\ H(\sigma) & E(\sigma) \end{bmatrix} \begin{bmatrix} x_\delta^c \\ y_\delta \end{bmatrix}, \sigma \in S \tag{1.9}$$

In point designs all the controller dimension must be the same.

Controller interpolation All the controllers can be represented as an indexed collection,

$$\begin{bmatrix} \dot{x}_\delta^c \\ u_\delta \end{bmatrix} = \begin{bmatrix} F^k & G^k \\ H^k & E^k \end{bmatrix}, k = 1, \ldots, K \tag{1.10}$$

Generally, there exists two controller interpolation methods. One method is to interpolate state-space controller coefficients. For example, a coefficient matrix $F(\sigma)$ is varied smoothly for $\sigma \in S$ and satisfy $F(\sigma_k) = F^k$, $k = 1, \cdots, k$. The other method is to interpolate the parameters of transfer functions. For example, controller transfer functions are interpolated by linear interpolation of poles, zeros, and gains [1].

Controller Scheduling It is different from previous point design approach that this scheduling approach is used to obtain the parameter-dependent controller directly. A general form controller for the nonlinear plant (1.1) can be written as follows,

$$\begin{aligned} \dot{x}^c &= f(x^c, y, w) \\ u &= h(x^c, y, w) \end{aligned} \tag{1.11}$$

An existing conclusion in control field is that if a nonlinear plant and nonlinear controller both have equilibria at the origin, then the corresponding closed-loop system has an equilibrium at the origin. And the linearization of the closed-loop system about the origin can be calculated as the closed–loop system for the linearized plant and linearized controller [1]. This conclusion also holds at nonzero equilibria. Obviously, in order to obtain satisfactory control effect for the nonlinear plant the condition that the equilibrium family of the controller (1.11) match the plant equilibrium family is required. Thus, it requires,

$$\begin{aligned} 0 &= f(x_e^c(\sigma), y_e(\sigma), w_e(\sigma)) \\ u_e(\sigma) &= h(x_e^c(\sigma), y_e(\sigma), w_e(\sigma)),\ \sigma \in S \end{aligned} \tag{1.12}$$

And the controller also need to satisfy the requirement which is the linearization for the controller (1.11) at each equilibrium is exactly the linear controller (1.9) at that equilibrium. Thus,

$$\begin{aligned} \frac{\partial f}{\partial x^c}(x_e^c(\sigma), y_e(\sigma), w_e(\sigma)) &= F(\sigma) \\ \frac{\partial h}{\partial y}(x_e^c(\sigma), y_e(\sigma), w_e(\sigma)) &= E(\sigma),\ \sigma \in S \end{aligned} \tag{1.13}$$

A common used controller family which meets the previous two requirements (1.12) and (1.13) is,

$$\begin{aligned} \dot{x}^c &= F(\sigma)[x^c - x_e^c(\sigma)] + G(\sigma)[y - y_e(\sigma)] \\ u &= H(\sigma)[x^c - x_e^c(\sigma)] + E(\sigma)[y - y_e(\sigma)] + u_e(\sigma) \end{aligned} \tag{1.14}$$

Because σ depends on the exogenous scheduling variable w and the measured output y the following equation is obtained,

$$\sigma(t) = g(y(t), w(t)) \tag{1.15}$$

Thus, the final gain scheduled controller is,

$$\begin{aligned} \dot{x}^c &= F(g(y,w))[x^c - x_e^c(g(y,w))] + G(g(y,w))[y - y_e(g(y,w))] \\ u &= H(g(y,w))[x^c - x_e^c(g(y,w))] + E(g(y,w))[y - y_e(g(y,w))] + u_e(g(y,w)) \end{aligned} \tag{1.16}$$

Direct design methods

LPV design method Consider the LPV plant,

$$\begin{bmatrix} \dot{x} \\ z \\ y \end{bmatrix} = \begin{bmatrix} A(\sigma(t)) & B_1(\sigma(t)) & B_2(\sigma(t)) \\ C_1(\sigma(t)) & D_{11}(\sigma(t)) & D_{12}(\sigma(t)) \\ C_2(\sigma(t)) & D_{21}(\sigma(t)) & 0 \end{bmatrix} \begin{bmatrix} x \\ v \\ u \end{bmatrix} \tag{1.17}$$

where,

$$\sigma(t) = \begin{bmatrix} \sigma_1(t) & \sigma_2(t) & \dots & \sigma_p(t) \end{bmatrix}^T \tag{1.18}$$

$$\sigma(t) \in S \subset \Re^p \tag{1.19}$$

$$\dot{\sigma}(t) \in R \subset \Re^p \tag{1.20}$$

$$S = \{\sigma \in \Re^p : |\sigma_i(t)| \leq \bar{\sigma}_i\} \tag{1.21}$$

$$R = \{\rho \in \Re^p : |\dot{\sigma}_i(t)| \leq \bar{\rho}_i\} \tag{1.22}$$

$\bar{\sigma}_i$ and $\bar{\rho}_i$ are pre-specified bounds, $i = 1, \ldots, p$.

Assume an LPV controller,

$$\begin{bmatrix} \dot{x}^c \\ u \end{bmatrix} = \begin{bmatrix} F(\sigma(t), \dot{\sigma}(t)) & G(\sigma(t), \dot{\sigma}(t)) \\ H(\sigma(t), \dot{\sigma}(t)) & E(\sigma(t), \dot{\sigma}(t)) \end{bmatrix} \begin{bmatrix} x^c \\ y \end{bmatrix} \tag{1.23}$$

The closed-loop system is obtained according to the LPV plant (1.17) and the LPV controller (1.23),

$$\begin{bmatrix} \begin{pmatrix} \dot{x} \\ \dot{x}^c \end{pmatrix} \\ z \end{bmatrix} = \begin{bmatrix} A_{cl}(\sigma(t), \dot{\sigma}(t)) & B_{cl}(\sigma(t), \dot{\sigma}(t)) \\ C_{cl}(\sigma(t), \dot{\sigma}(t)) & D_{cl}(\sigma(t), \dot{\sigma}(t)) \end{bmatrix} \begin{bmatrix} \begin{pmatrix} x \\ x^c \end{pmatrix} \\ v \end{bmatrix} \tag{1.24}$$

Considering the induced norm of the mapping from the exogenous signals to the error signals as the closed-loop performance, i.e. $||T_{zv}||$. If the induced norm satisfies

$$||T_{zv}|| < \gamma \tag{1.25}$$

and the corresponding unforced closed-loop system is exponentially stable then a controller is considered to achieve a performance of γ.

Following theorem describes a sufficient condition to achieve closed-loop perfor-

mance.

Theorem 2 *A controller achieve a performance level of γ if there exists $X(\sigma) = X^T(\sigma) > 0$ such that*

$$\begin{bmatrix} X(\sigma)A_{cl}(\sigma,\rho) + A_{cl}^T(\sigma,\rho)X(\sigma) + \sum_{i=1}^{p} \frac{\partial X(\sigma)}{\partial \sigma_i}\rho_i & X(\sigma)B_{cl}(\sigma,\rho) & \gamma^{-1}C_{cl}^T(\sigma,\rho) \\ B_{cl}^T(\sigma,\rho)X(\sigma) & -I & \gamma^{-1}D_{cl}^T(\sigma,\rho) \\ \gamma^{-1}C_{cl}(\sigma,\rho) & \gamma^{-1}D_{cl}(\sigma,\rho) & -I \end{bmatrix} < 0 \tag{1.26}$$

for all $\sigma \in S$ and $\rho \in R$.

(1.26) can be transformed to an LMI form, and then a LPV controller can be obtained.

LFT design method An LPV plant with LFT parameter dependence can be written as follows [1],

$$\begin{bmatrix} \dot{x} \\ z_\sigma \\ z \\ y \end{bmatrix} = \begin{bmatrix} A & B_\sigma & B_1 & B_2 \\ C_\sigma & D_{\sigma\sigma} & D_{\sigma 1} & D_{\sigma 2} \\ C_1 & D_{1\sigma} & D_{11} & D_{12} \\ C_2 & D_{2\sigma} & D_{21} & 0 \end{bmatrix} \begin{bmatrix} x \\ v_\sigma \\ v \\ u \end{bmatrix} \tag{1.27}$$

where, z_σ and v_σ are "artificial" signals with

$$v_\sigma = \Delta(\sigma) z_\sigma \tag{1.28}$$

and,

$$\Delta(\sigma) = diag(\sigma_1 I_{n1}, \sigma_2 I_{n2}, \cdots, \sigma_p I_{np}) \tag{1.29}$$

The corresponding controller with LFT parameter dependence can be written as follows,

$$\begin{bmatrix} \dot{x}^c \\ u \\ u_\sigma \end{bmatrix} = \begin{bmatrix} F & G_1 & G_\sigma \\ H & E_{11} & E_{1\sigma} \\ H_\sigma & E_{\sigma 1} & E_{\sigma\sigma} \end{bmatrix} \begin{bmatrix} x^c \\ y \\ y^\sigma \end{bmatrix} \tag{1.30}$$

where,

$$u_\sigma = \Delta(\sigma) y_\sigma \tag{1.31}$$

The key point in the LFT design method is that all σ dependence is contained in $\Delta(\sigma)$. i.e. the parameter variations are seen as "unknown perturbations" on an time-invariant system. Thus, time-invariant controller design method can be used to design the controller. After the design, the parameter variations are incorporated in the time-invariant controller to produce the final LPV controller.

1.2.2 Gain scheduling of controller switching or blending

Gain scheduling in the sense of controller switching or blending means that various controllers are designed for various local models and then the controller output is chosen as a combination of the actions or parameters of the local models or controllers.

Normally, the controller design approach consists of the following steps:

- Partition the system's full operating range into several operating regimes in according to the practical situation.
- Obtain a local model for each operating range.
- Design a controller for each local model.
- Combine the local models or controllers into a global one.

The core of this strategy is to make use of a partitioning of the operating space of the plant in order to solve modelling and control problems [2]. Normally, for

different operating points the different local models or local controllers are used, and a supervisor is used to coordinate the multiple models or multiple controllers. Figure 1-1 shows the architecture of this strategy. Different methods in modeling, controller designing and switching strategy are given by researchers. Correspondingly, there exist several gain scheduling methods in the sense of controller switching or blending. In terms of modeling; there exists different model structures by which the global model can be approximated, e.g. piecewise models, fuzzy models and neural network models, adaptive models etc. In terms of controller design; if a simple local model is obtained, a variety of conventional controller design methods can be used, e.g. PID, LQR, GPC, MPC and H_∞ controller etc. In terms of switching strategy; there are mainly two categories of logic switching, i.e. nonestimator-based supervisors and estimator-based supervisors. In all of these various methods stability is a difficult issue to analyze. An input-output approach, a novel controller switching technique, is presented in [3]. System stability is the main design objective of the input-output approach. All previous controller design methods are put into four categories according to different design principles. The four categories are combination of local controller outputs, global model based controller, logic-based switching and an input-output approach.

1.2.2.1 Combination of local controller outputs

The schematic combination of local controller output is shown in Figure 1-2. The multiple local linear or nonlinear models are obtained for the different operating regimes. Controllers are designed according to local models. In this approach the scheduling variables should be decided. The final controller outputs are obtained by interpolating between the individual controller outputs based on the weights. According to the value of the scheduling variable, the different weights for the local controllers outputs are used.

The main advantage of this approach is that the switching among different controllers is smooth because the global controller output is composed of the interpola-

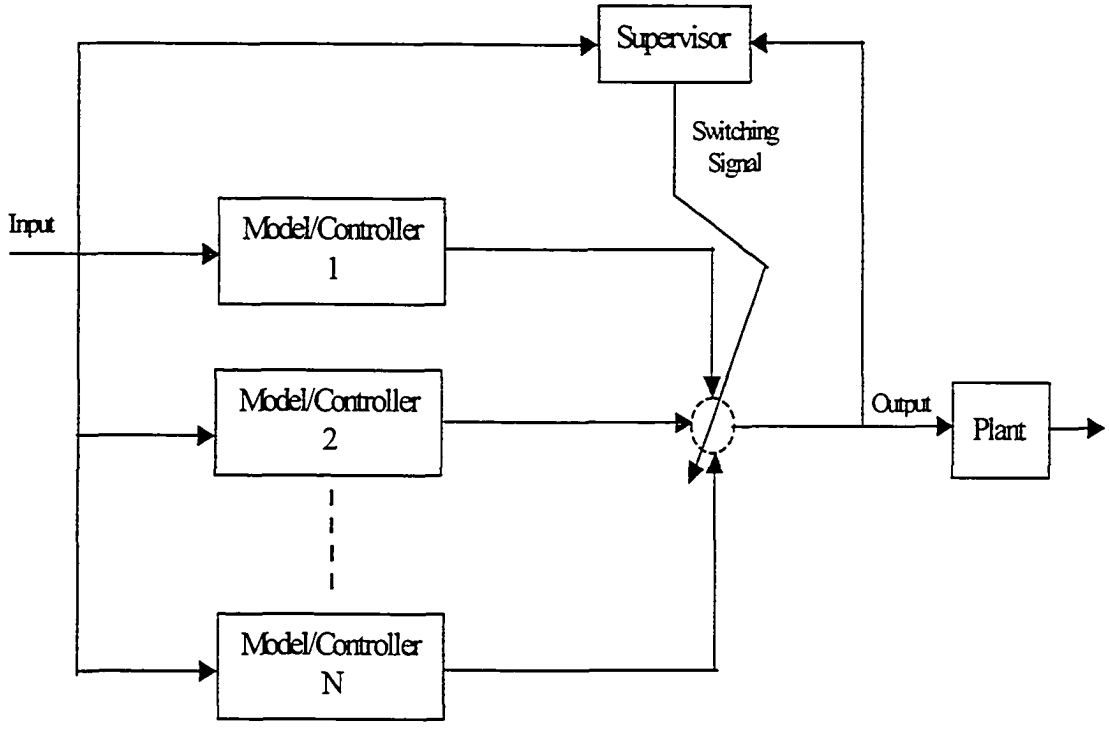

Figure 1-1: Architecture of the multiple model/controller approach

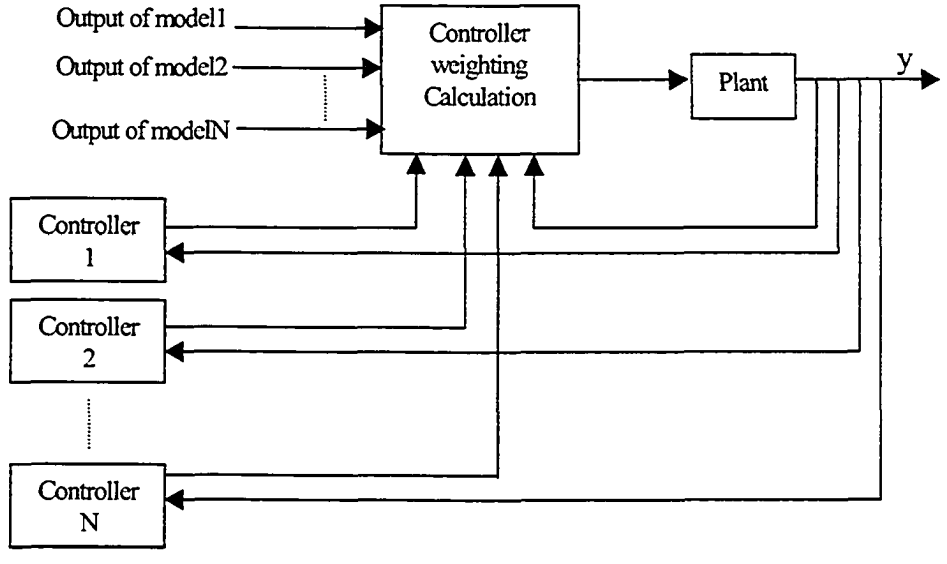

Figure 1-2: Schematic of combination local controller output approaches

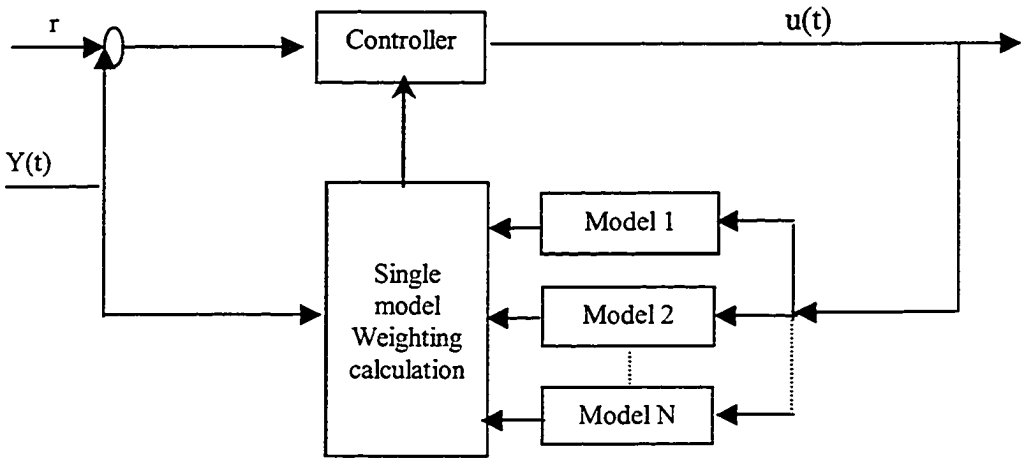

Figure 1-3: Schematic of global model based controller

tion of the output of local controllers, rather than directly switch among the local controller output.

In [4], Dougherty and Cooper use the first-order plus dead time (FOPDT) model to approximate the nonlinear plant, and design corresponding DMC controllers for each local model. One measured process variable is used as scheduling variable to decide the different weights for calculating the global controller output.

In [55], Omar et al employ multiple first-order linear models to approximate the nonlinear plant. H_∞ controller design method is used to design corresponding linear controllers. Multiple filters are devised to weight the outputs of the local controllers.

1.2.2.2 Global model based controller

An alternative approach is to exploit the global model based on the local models. Then a controller is designed based on the global model. This approach has several advantages. The main advantage is that the system is controlled by a global controller, which is expected to give better plant-wide control performance simply because global information can be applied to determine the control input [2]. Figure 1-3 shows a schematic of this approach.

In [5] Gendron et al use the first-order plus dead-time (FOPDT) model to obtain the local models. In [6] Foss et al. develop the simple nonlinear model to approximate the plant. They all construct the global model via a weighted sum of local multiple models. The weight is calculated according to the model prediction error, with the larger weights corresponding to smaller model prediction errors. Thus a global model is obtained. In [5] a PID controller is designed. In [6] nonlinear model predictive controller is used to control the global model. In [7] the operating space is decomposed into a set of local models which form a network. Then the local models are combined into a global model structure using an interpolation method based on normalized basis functions. The MPC algorithm is used to design the controller in [7].

1.2.2.3 logic-based switching

The previous two methods either used a combination of local controller outputs or the combination of local models. Since 1991 researchers at Yale University have investigated controller design using logic-based switching. In logic-based switching method the multiple linear models are obtained for different operating regimes, and corresponding linear controllers are designed respectively, finally the supervisor is devised to orchestrate the switching among the candidate controllers [8]. Obviously the overall systems of the logic-based control are hybrid dynamic systems. The schematic of logic-based switching control is showed in Figure1-4.

Generally there are two categories of the logic-based switching control system considering the different supervisor algorithms, one is nonestimator-based supervisor and the other is estimator-based supervisor.

Nonestimator-based supervisor A nonestimator-based supervisor is also called a prerouted parameter tuner which moves a switching signal σ along a prespecified path and only decides if and when or how fast to change the switching signal. The input of the nonestimator-based supervisor is a tuning error e which is a linear function of the measurable signals in the sub-system. The output of the nonestimator-based

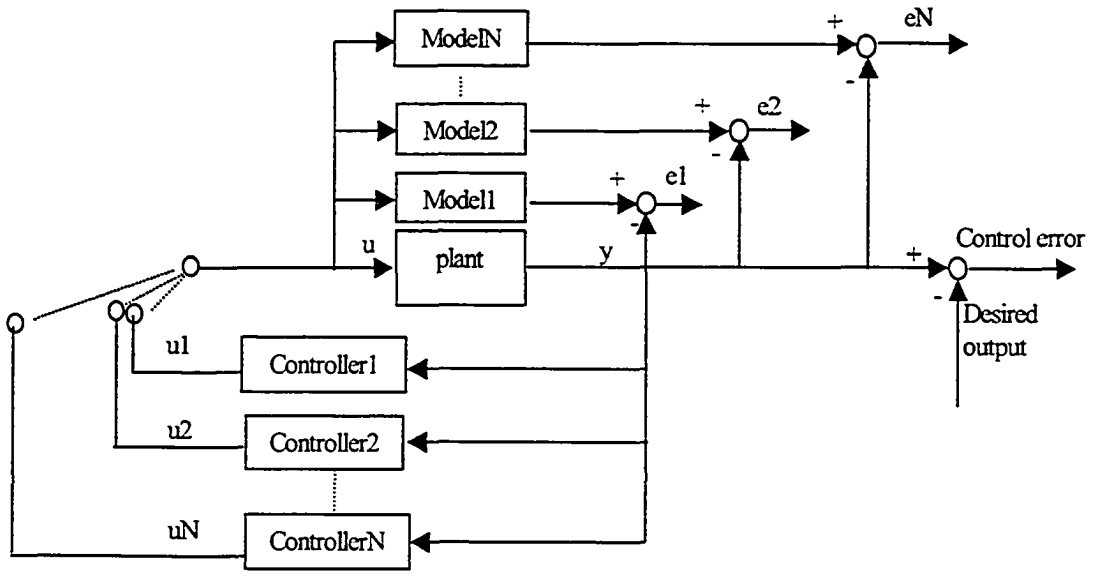

Figure 1-4: Schematic of logic-based switching control

Figure 1-5: Nonestimator-based supervisor

supervisor is the switching signal σ. Figure 1-5 shows the block diagram of the nonestimator-based supervisor.

There are a number of different ways to realize the nonestimator-based supervisor, but basically they have the similar logic. Figure 1-6 shows the flow chart of a common nonestimator-based supervisor.

In flow chart Figure 1-6 π is a piecewise-continuous performance signal which directly relate with the tuning error e as follows,

$$\dot{\pi} = ||e||^2 \tag{1.32}$$

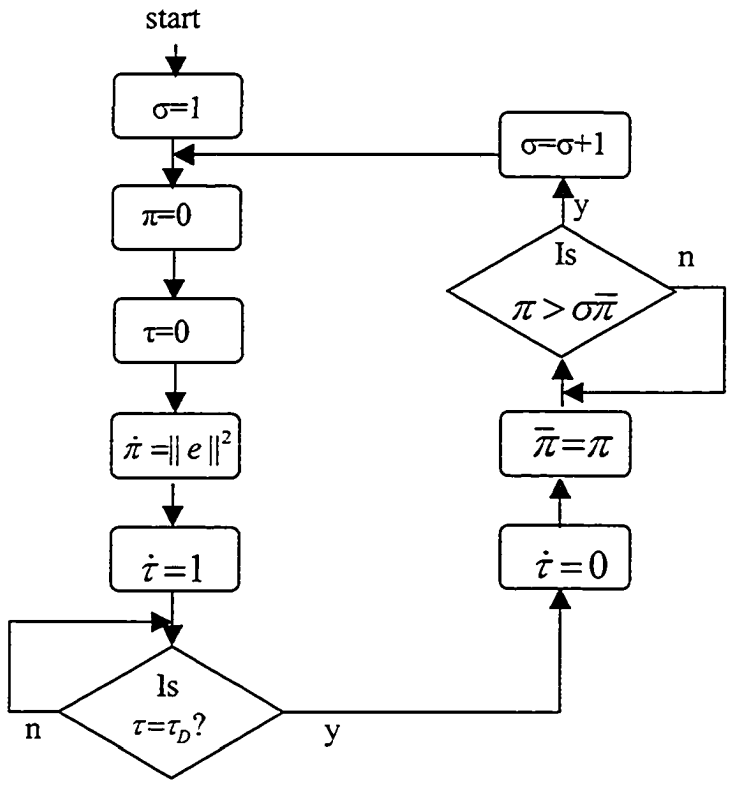

Figure 1-6: Flow chart of a nonestimator-based supervisor

$\bar{\pi}$ is sampled performance signal, τ is a timing signal, τ_D is a preselected positive number called dwell time. Once the algorithm is started the supervisor waited until the dwell time length τ_D is elapsed, $\bar{\pi}$ is set equal to the value of π, if π is less than or equal to $\sigma\bar{\pi}$ the performance signal π just update by the equation (1.32), if π is greater than $\sigma\bar{\pi}$ the switching signal is increased by 1. Here, the dwell time τ_D is used to avoid the infinitely fast switching i.e. chattering.

Estimator-based supervisors An esitmator-based supervisor is devised to decide when and which controller should be used. The schematic of the estimator-based supervisor is shown in Figure 1-7. Estimator $P_1, P_2, \cdots P_m$ are corresponding estimators for multiple models, the output $y_{p1}, y_{p2}, \cdots y_{pm}$ are the corresponding estimated outputs for multiple models, $e_{p1}, e_{p2}, \cdots e_{pm}$ are the corresponding output estimation errors for the multiple models, $\pi_{p1}, \pi_{p2}, \cdots \pi_{pm}$ are the corresponding performance signals which are closely related with the corresponding output estimation errors, Σs is a supervisor to decide the switching signal σ. The idea behind the estimator-based supervisor is: the model which gives the smallest performance signal can represent the current plant best, thus the controller which is designed for this model can be employed for the plant. According to this idea the task of the supervisor is to find the smallest performance signal and then make the correct switching.

There are several methods to realize the estimator-based supervisor. In generally, all the methods can be classified into two approaches, one is hysteresis switching, and the other is dwell-time switching.

The flow chart of the hysteresis switching can be shown in Figure 1-8. In this flow chart h represents hysteresis constant, q is the positive integer set {1,2, ... m}. The flow chart shows the switching will not immediately occur until the condition $\pi_q + h < \pi_\sigma$ is satisfied. The main function of the hysteresis constant h is to avoid chattering. The disadvantage of this switching approach is that the minimum time between switching is often unknown a priori [9].

The flow chart of the dwell-time switching is shown in Figure 1-9. In this flow

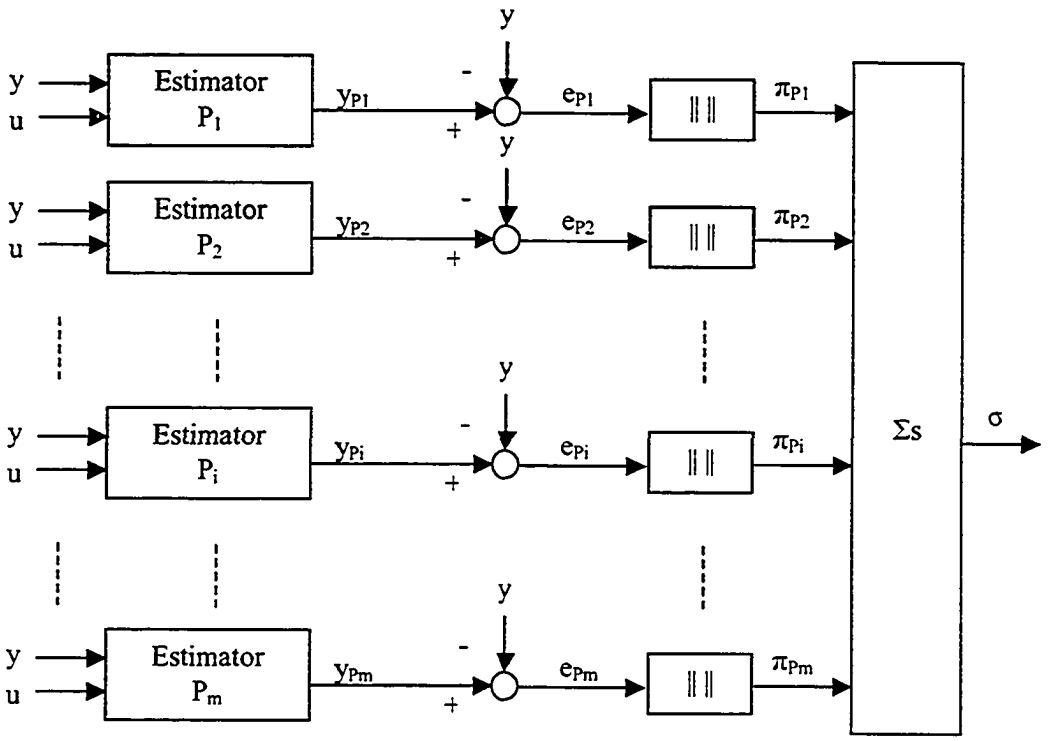

Figure 1-7: Schematic of the estimator-based supervisor

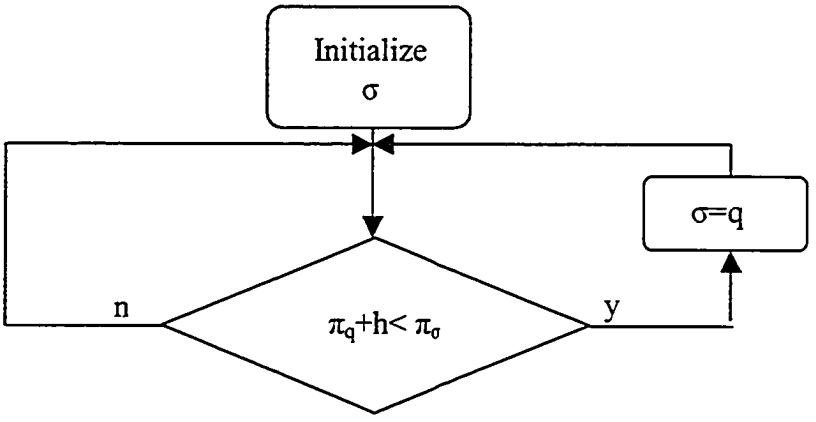

Figure 1-8: Flow chart of the hysteresis switching

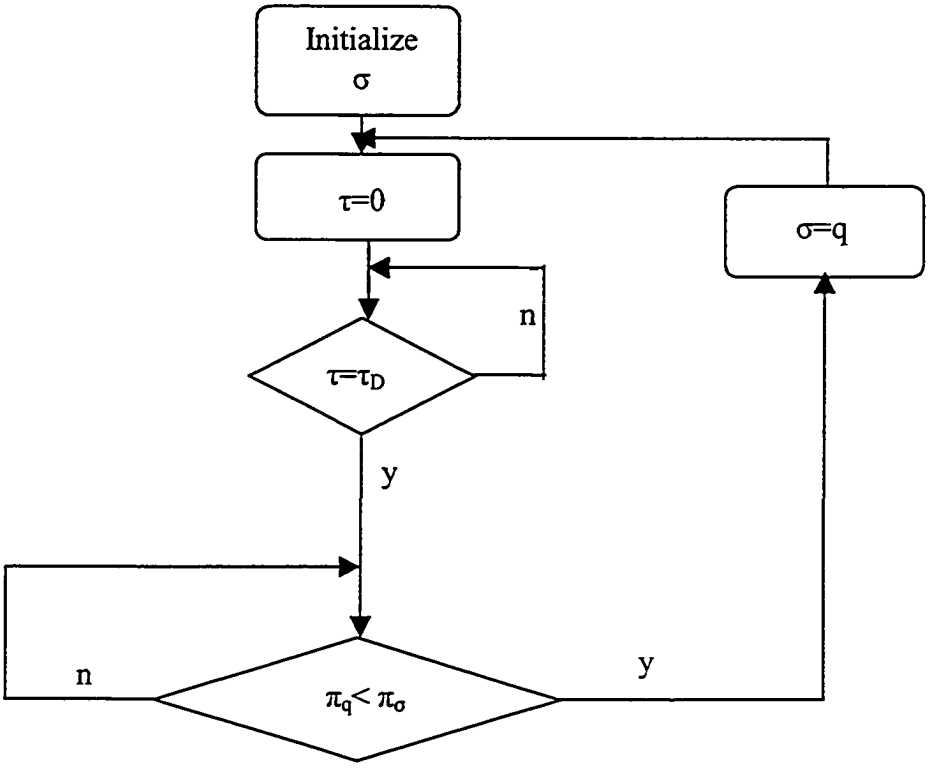

Figure 1-9: Flow chart of the dwell-time switching

chart τ is a timing signal which takes values in the interval $[0, \tau_D]$, τ_D is dwell time. The dwell-time switching works as follows, after each switching signal changed the switching signal will be held for the fixed time τ_D, after the dwell time τ_D elapsed the supervisor will check whether the condition $\pi_q < \pi_\sigma$ is satisfied, only if the condition is satisfied the switching signal will changed. Obviously, τ_D is used to avoid the chattering.

In [10][11] Narendra et al used a mixture of fixed models and adaptive models to approximate the plant: a Neural Network is employed to realize the identification and controllers. The performance index, is closely related with the model prediction error. The controller that achieves the smallest performance index is selected to control the plant. The hysteresis switching algorithm is used. In [12] LPV model is used to represent the local models. Corresponding robust H_∞ controller is used to

achieve robust stability and robust performance. The dwell-time switching algorithm is employed.

1.2.2.4 An input-output approach

A novel input-output approach is presented in [3]. This approach reformulate the theory of input-output systems presented by Sandberg and Zames. Unlike previous methods, this approach focuses on ensuring system stability. It was proved that if a "stable motion" is established the system is stable. The work of this thesis is mainly based on the results of this approach. The approach is introduced as follows.

Similar as methods which are introduced in Section 1.2.2, multiple local models at different operating regimes should be obtained first. The state space realization of the nonlinear plant is as follows,

$$\dot{x}(t) = f(x, u),\ u \in \chi \tag{1.33}$$

$$y(t) = h(x) \tag{1.34}$$

where,

x represents the state vector and $x \in R^n$, u represents the input function and χ represents an abstract function space to be defined.

Following notation will be used in the rest part of this section,

$x(t, t_0, x_0, u)$ represents the state trajectory which starts at initial time $t = t_0$ with initial condition $x(t_0) = x_0$. $\Omega \subset R^+$ have the form $\Omega = [t_1, t_2]$ or $\Omega = [t_1, \infty)$. Z denotes the linear space of measurable functions $z : \Omega \rightarrow R^q$. χ is defined as:,

$$\chi = \{u \in Z : ||\cdot||_\infty < \infty,\ and\ ||\cdot||_2 < \infty\}$$

where,

$||\cdot||_\infty$ and $||\cdot||_2$ are the L_∞ norm and L_2 norm respectively. $\chi([t_0, t_1])$ represents

that χ is defined $\forall t \in [t_0, t_1]$. χ_e is the extension of the space χ. u_T is used to denote the truncation of the input function u which is defined as follows,

$$u_T(t) = \begin{cases} u(t), & if\ t \leq T \\ 0, & if\ t > T \end{cases}$$

χ_Q is used to define the subset of χ, $\chi_Q = \{u \in \chi : ||u||_\infty < Q\}$. The set of bounded motions in state space as χ_α is defined as,

$$\chi_\alpha = \{x \in \chi([0, \infty)) : ||x(t)||_\infty < \alpha\}$$

The pair (x_e, u_e) is used to denote an equilibrium point of the system (1.33) and (1.34), Thus,

$$f(x_e, u_e) = 0 \quad \forall t \geq t_0$$

In traditional input-output theory the functional relation between inputs and outputs is studied. The disadvantage of this theory is that the effect of initial condition is unable to be considered since the system should be assumed relaxed. To avoid the shortcoming a system is considered as a mapping from input to state in [3]. In order to explain the new input-output theory the definition of the local models is given as follows.

Definition 3 *For a given physical system, a local model about (x_e, u_e), denoted $H[x_e, u_e]$, is a pair of functions f, h such that*

$$\begin{aligned} \dot{x}(t) &= f(x, u) \quad t, t_0 \in R^+,\ t \geq t_0, (u - u_e) \in \chi_Q, |x_0 - x_e| \leq \alpha \qquad (1.35) \\ y(t) &= h(x) \in \chi_e \end{aligned}$$

Here, a local model is considered as a mapping from $\chi_Q \rightarrow \chi_e$, hence whenever $x(t)$ is a bounded subset of χ_e $H[x_e, u_e]$ is considered be locally stable, and the accurate mathematics definition is as follows,

Definition 4 *$H[x_e, u_e]$ is said to be locally stable if*

$$u - u_e \in \chi_Q, |x_0 - x_e| \leq \alpha \Longrightarrow (x - x_e) \in x_\alpha$$

Assuming the control problem is to move the state of system from x_0 to a final state x_f, at $t = t_f$. An important concept, stable motion, is presented in [3]. The definition is as follows,

Definition 5 *A system is said to experience a stable motion from an initial state x_0 at $t = 0$ to a final state x_f at $t = t_f$ if the following conditions are satisfied:*

1. $\exists m$ *locally stable models* $H[x_{ei}, u_{ei}]$, $i = 1, 2, \cdots, m$ *with* $x_0 \in A_1$ *and* $x_f \in A_m$;

2. For each $t = t^*$ *we have:*

(a) $x(t^*) \in A_k$ *for some* $k = 1, 2, \cdots, m$;

(b) $\exists \varepsilon > 0 : (u(t)) - u_{ei}(t)) \in \chi([t, t^*])_{Qk}\ t^* \leq t \leq t^* + \varepsilon$

This concept is a generalization of the concept of stability along a trajectory in the sense of Lyapunov. Based on this definition the author of [3] provides a theorem which can be used to ensure the stability of the multiple model system. The theorem is as follows,

Theorem 6 *Consider a physical system and m local models $H[x_{ei}, u_{ei}]$, $i = 1, 2, \cdots, m$. If following conditions are satisfied, then it is possible to steer the system from an initial state $x_0 \in R^n$ to a final state $x_f \in R^n$ at $t = t_f$ following a stable motion.*

1. $x_0 \in A_1, x_f \in A_m$

2. $A_i \cap A_{i+1} \neq \emptyset, i = 1, 2, \cdots, m - 1$

The idea behind the above theorem can be explained by the Figure 1-10, here two states are used to show the principle of the theorem, in actual case there maybe exists system states more than two. The control objective is to steer the system state from $x(t_0)$ to $x(t_f)$. Each of the sets A_i represents a region of the state space where a local linear model can be used to design a controller that guarantees both stability

and performance. The operating region of each controller defines the boundary of the operating region for each local model. Without a switching mechanism, system trajectories would be confined to one and only one operating region A_i. In order to enlarge to operating region, multiple models are obtained in such a way that there is an overlap between 2 neighbor regions. Switching between two adjacent models and corresponding controllers are implemented when a system trajectory reaches the intersection of two neighbor regions. In Figure 1-10 there exists overlapping area between any neighbored local model areas. $x(t_1), x(t_2) \cdots$ are the points at which the controller is switched. This picture clearly shows the idea of [3]: the initial point of the system states is $x(t_0)$, since the local model is controllable some control input function u corresponding to the model A_1 can always be found to move the system states to the overlapping area which is the common region of model A_1 and model A_2, when system states achieve the point $x(t_1)$ the controller which is designed for the model A_2 will be used, then some control input function u can be found to move the systems states to the next overlapping area which is the common area between model A_2 and model A_3, $\cdots$ so on so forth, until the system states are steered to the desired point $x(t_f)$. The stable motion in the whole control process is realized, thus the stability of the whole system is achieved.

1.3 Robust control

One important factor for obtaining a good controller is an accurate model of the plant, but in practical application it is very difficult to obtain an accurate model, thus the model always comes with some uncertainties, this motives the research interest to design controller for models with uncertainties, i.e. robust control theory. Researchers made lots of efforts to study robust controller design [13]. From 1927 to present a large number of related papers were published. In general there are three periods for the robust control theory study, i.e. classical sensitivity design period, state-variable period and modern robust control period [13].

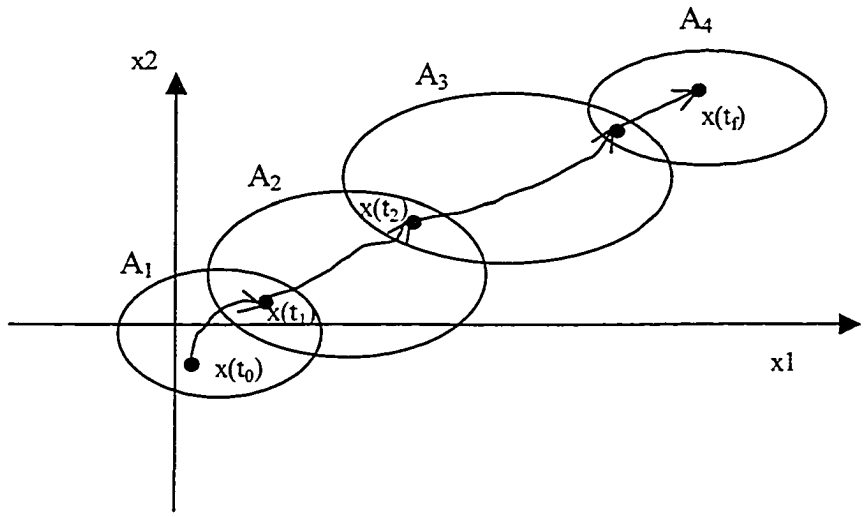

Figure 1-10: Stable motion of system states

The period from 1927 to 1960 is the classical sensitivity design period in which loop shaping of single-input single-output (SISO) systems for stability, sensitivity reduction and noise suppression is the main research interest of the robust control [13]. The earliest solution of robust control problem can trace back to 1927 when H.S. Blace presented large-loop gain to overcome the significant plant uncertainties. In 1932 Nyquist provided the relation between dynamic stability and large-loop gain. In 1945 Bode presented the differential sensitivity function.

During the period from 1960 to 1975 the state-space theory was developed. Cruz and Perkins presented the concept of the sensitivity comparison matrix in 1964 for multiple-input multiple-output (MIMO) systems, actually it extended SISO sensitivity results to MIMO systems. In 70's some further results of the sensitivity problem were reported.

The period from 1975 to present is the modern control period in which significant results were reported [13]. Youla et al. and Desoer et al. introduced the concept of coprime matrix fraction description of MIMO systems in 1976 and 1981 respectively. Rosenbrock, MacFarland and Postlethwaite extended the Nyquist stability

criterion to MIMO systems. Youla et al also introduced the parameterization of all stabilizing compensators which is called Youla parameterization. Safonov and Athans generalized gain and phase margins to MIMO systems in 1977. At that time a large number of a multivariable robust design approaches of optimal LQ and LQG were also developed. In 1980 Safonov gave the sector-type stability criterion which was a generalization of the conic sector stability concepts introduced by Zames. In 1981 a number of results of singular values are presented. Doyle presented the concept of the structured singular value in 1982. In 1983 Zames and Francis introduced the optimal H_∞ sensitivity design problem, they use the optimal Nevanlinna-Pick interpolation theory to solve this problem. In 1984 different researchers provided solutions to the MIMO optimal H_∞ sensitivity problem. In 1985 Youla and Bongiorno gave a solution to the H_2 optimal sensitivity design problem.

In this thesis the controller design for a cogeneration system based on the multiple model approach of reference [3] is investigated.

Chapter 2

Model of the Utility boiler system

2.1 Background

The Syncrude Canada Ltd. (SCL) cogeneration system consists of three identical utility boilers (UB), two identical carbon monoxide (CO) boilers and two identical once-through steam generators (OSTG), four headers which have different pressure levels (6.306MPa, 4.24MPa, 1.068Mpa and 0.372MPa). The 6.306MPa header receives steam from UBs, COs and OTSGs, and the steam is distributed through the header system, some steam is used to generate electricity, some is used for extracting, heating and upgrading. Figure 2-1 shows the diagram of the cogeneration system.

Since the steam is used for generating electricity and process application the demand for the steam is variable, but the same steam quality should be provide in any situation in order to keep the normal plant operation. Thus, the control objective of the cogeneration system is to track the steam demand while maintain the steam pressure and the steam temperature of the 6.306MPa header at their respective setpoints [18]. In SCL the utility boilers are used to control the steam pressure and steam temperature. Currently multiloop proportional plus integral (PI) controllers are used to control the utility boilers. When steam demand is changed the transient response of the 6.306 MPa header exhibits oscillatory modes, sometimes even make the complete

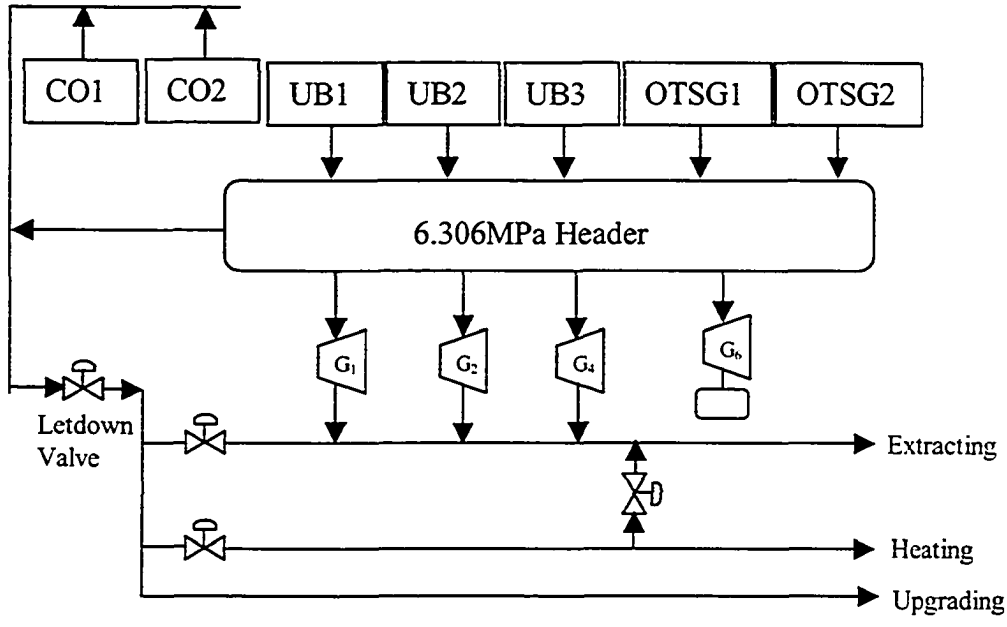

Figure 2-1: Diagram of the cogeneration system

plant shutdown. Thus the main work of this thesis is to redesign the controller so that the utility boiler system keep stability and reach the desired performance.

2.2 Utility Boilers

The utility boilers in the SCL are watertube drum boilers. The scheme of the utility boiler is shown in Figure 2-2.

First, cold water is fed into the utility boiler, before cold water enter into the steam drum economizer is used to preheat feedwater so that the temperature of the cold water increases from about 141 $^{\circ}C$ to 184 $^{\circ}C$. Water after economizer is so called subcooled water. The subcooled water in the steam drum flows through the downcomers, and goes into the mud drum in which the subcooled water is distributed into the waterwalls and the risers. The water in waterwalls and the risers receives radiant heat and produces steam which causes the steam-water mixture in risers and downcomers since the density of the subcooled water and saturated steam-water are

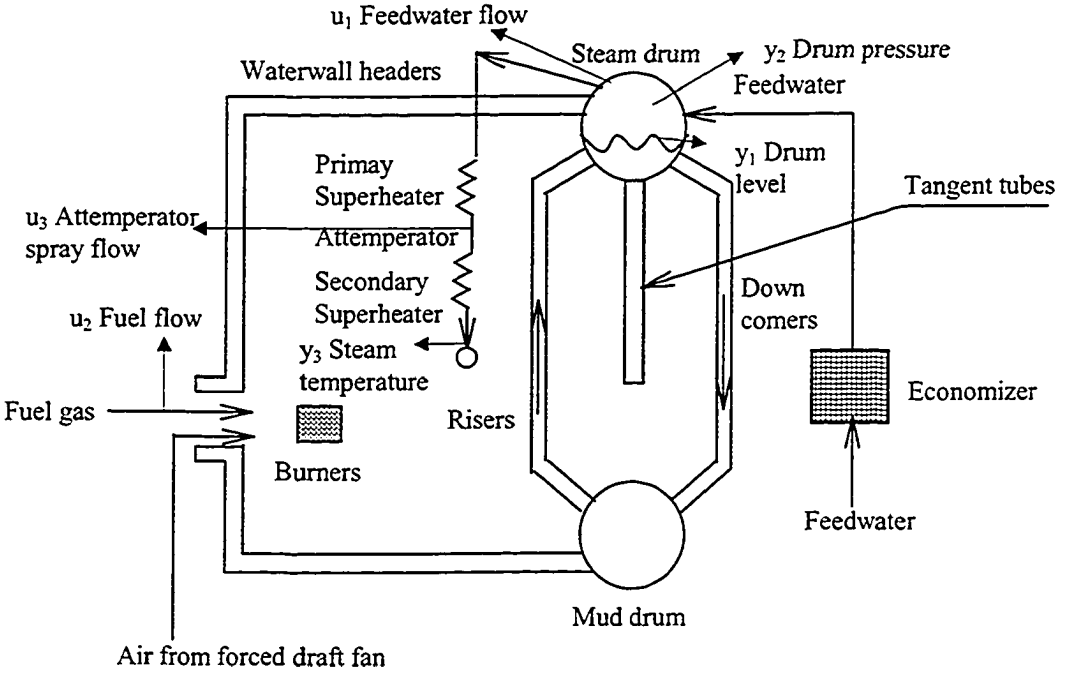

Figure 2-2: Scheme of a utility boiler

different. Naturally, the circulation of the steam-water mixture in risers and downcomers is formed. Thus, the saturated steam-water mixture enter into the steam drum, in which the steam is separated from the water. The saturated steam then enters into the primary superheaters and the secondary superheaters. An attemperator is in between the primary superheater and the secondary superheater. In attemperator the steam in the primary superheater is mixed with the subcooled water so that to adjust the temperature of the steam in the secondary superheater.

2.3 Utility Boiler model

The work in [15][16][17][18][19] shows that it is very complex to obtain the utility boiler model using the first principle methods. Even though a model can be obtained by the first principle method, it is difficult to design a controller for such a model due to model complexity. Thus, in this thesis the model identification technique is used to obtain the model. Unfortunately, the utility boiler exhibits strongly nonlinearity. No single linear model can describe such severe nonlinear plant accurately. Therefore, multiple model technique is used to represent the utility boiler system. The idea of multiple model method is to decompose the entire operating range of the system into several operating regimes. Local models for the sub operating regimes are simpler than global model. Correspondingly, the controller design for the local models will be simpler than that for the global model. Hence, the complex control problem can be transformed into several simpler problems by using multiple model technique.

All of the results reported have been simulated using SYNSIM. SYNSIM is a nonlinear simulation package developed in a collaboration between the University of Alberta and Syncrude Canada with the purpose of studying certain upset conditions sporadically observed in the plant, as well as a general tool for stability and performance analysis. This package has been extensively tested and is routinely used by Syncrude personnel. Correlation between measurements from the true plant and predictions by the model are considered excellent. Therefore, the simulation is considered

as a true measure of the controller response in the presence of the real plant.

A properly functioning boiler should meet the following requirements: (1) a certain steam pressure should be maintained at the outlet of the drum despite variations in the amount of steam demanded by users; (2) the water level in the drum should be kept at the desired level to avoid overheating of drum components or flooding of steam lines; (3) The steam temperature must be kept at a certain level to avoid overheating of the superheaters.

Thus, following principal variables are chosen as output of the utility boiler model:

y_1 *drum level* (m)

y_2 *drumpressure* (KPa)

y_3 *steam temperature* $(°C)$

Following principal variables are chosen as input of the utility boiler model:

u_1 *feedwater flow rate* (kg/s)

u_2 *fuel flow rate* (kg/s)

u_3 *attemperator spray flow rate* (kg/s)

Consequently, the utility boiler model is a 3×3 model.

2.3.1 Operating points selection

Since different models at different operating points should be obtained the suitable operating points are chosen first. The requirements for the operating points selection are as follows. First, the model obtained by the system identification method is always valid on a neighborhood of an operating point, and the entire operating space of the utility boiler is not only a small neighborhood of an operating point. Thus, enough operating points should be chosen so that all the operating space of the identified linear model can cover the entire operating space of the utility boiler. Second, the final objective is to obtain an appropriate multiple controllers that keep the system stability and reach the desired performance. According to [3] there should exist overlapping area between the neighbored linear model. Thus, there should exists the

overlapping area between neighbored operating spaces.

According to field experience the utility boiler system works mainly in three typical operating points, which are low load operating point, normal load operating point and high load operating point. The parameters of the different operating points are listed in Table 2.1.

	Low load	Normal load	High load
Steam flow rate	50.12 kg/s 397.43 $kpph$	68.94 kg/s 546.66 $kpph$	83.58 kg/s 662.75 $kpph$
Steady state values	$u_{10} = 50.12\ kg/s$ $u_{20} = 2.62\ kg/s$ $u_{30} = 0\ kg/s$ $y_{10} = 1\ m$ $y_{20} = 6523.6\ kpa$ $y_{30} = 483.19\ °C$	$u_{10} = 68.36\ kg/s$ $u_{20} = 3.67\ kg/s$ $u_{30} = 0.58\ kg/s$ $y_{10} = 1\ m$ $y_{20} = 6711.7\ kpa$ $y_{30} = 500\ °C$	$u_{10} = 81.74\ kg/s$ $u_{20} = 4.48\ kg/s$ $u_{30} = 1.84\ kg/s$ $y_{10} = 1\ m$ $y_{20} = 6894\ kpa$ $y_{30} = 500\ °C$

Table 2.1: Parameters of different operating points

Intuitively, it is reasonable if three linear models at above three operating points are identified, however whether the three operating points can meet the two conditions which are mentioned in pervious parts still should be checked. From Table 2.1 the variable ranges of u_1 and u_2 for the operating space changes from low load to normal load and from normal load to high load respectively can be calculated. Here u_3 is not considered since it is no solution for the variable rate when operating point move from low load to normal load, and fortunately the absolute value variation is small, hence the impact of u_3 is ignored. Table 2.2 shows the calculation result for the variation range of u_1 and u_2.

	Low load → Normal load	Normal load → High load
u_1	36%	20%
u_2	40%	22%

Table 2.2: The variation range of u1 and u2.

Then some experiments are conducted on the SYNSIM simulation package. 10%, 30% and 40% step changes of u_1 are given respectively at low load operating points.

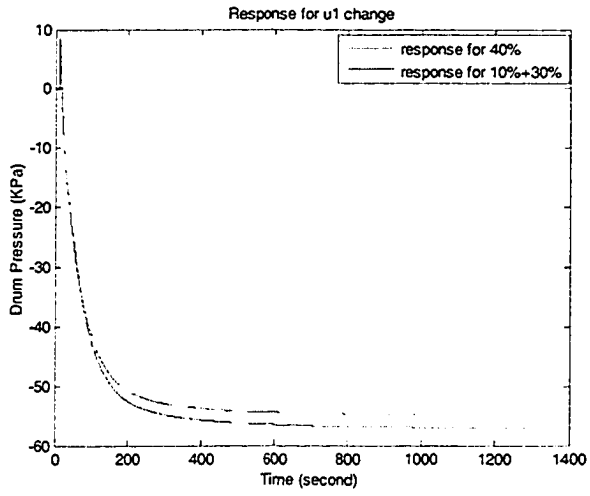

Figure 2-3: y_2 comparison results for additivity at low load operating point

And the corresponding outputs of y_2 and y_3 are recorded. The reason here the output of y_1 is not recorded is that the y_1 channel is an unstable channel. In order to check whether one liner model is enough when the u_1 changes 40% two curves are plotted respectively for y_2 and y_3. Figure 2-3 and Figure 2-4 shows the results, in which the dash line is the response to 40% variation of u_1, and the solid line is the sum of response to 10% and 30% variation of u_1 respectively.

Similarly, 10%, 30% and 40% step changes of u_2 are given respectively at low load operating point. And the corresponding outputs of y_2 and y_3 are plotted in Figure 2-5 and Figure 2-6.

Obviously y_2 response for 40% u_1 change roughly follows the same trend with the sum of y_2 response for 10% and 30% u_1 change, and y_3 response for 40% u_1 change roughly follows the same trend with the sum of y_3 response for 10% and 30% u_1 change, and y_2 response for 40% u_2 change roughly follows the same trend with the sum of y_2 response for 10% and 30% u_2 change, and y_3 response for 40% u_2 change roughly follows the same trend with the sum of y_3 response for 10% and 30% u_2 change. Thus, one linear model is enough to represent the original plant when u_1 and

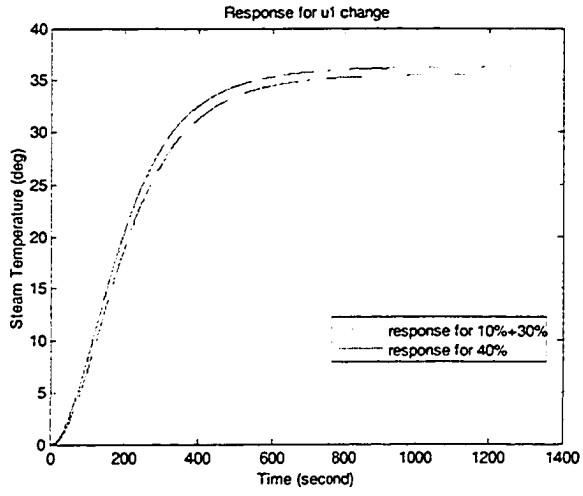

Figure 2-4: y_3 comparison results for additivity at low load operating point

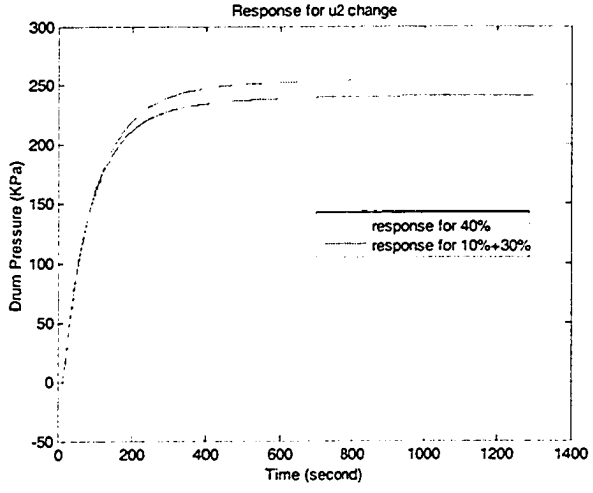

Figure 2-5: y_2 comparison results for additivity at low load operating point

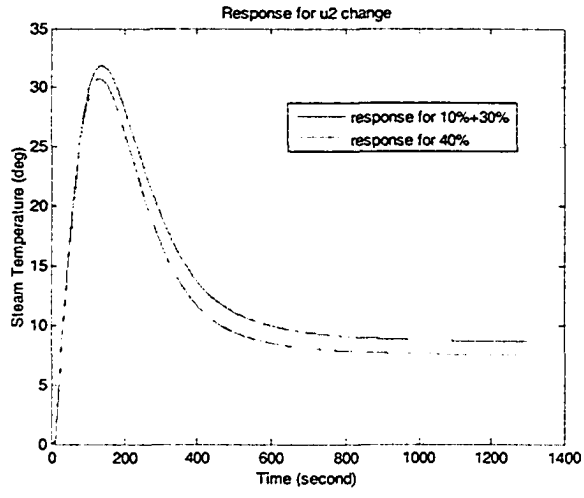

Figure 2-6: y_3 comparison results for additivity at low load operating point

u_2 change 40% respectively at low operating point, i.e. there is no need to add linear model in between low load operating point and normal load operating point.

Next, the linear area for the nominal operating point is checked. 5%, 15% and 20% variation of u_1 are given respectively at normal load operating point, and the corresponding outputs of y_2 and y_3 are plotted in Figure 2-7and Figure 2-8.

Similarly 5%, 15% and 20% variation of u_2 are given respectively at normal load operating point, and the corresponding outputs of y_2 and y_3 are plotted in Figure 2-9 and Figure 2-10.

Clearly y_2 response for 20% u_1 change roughly follows the same trend with the sum of y_2 response for 5% and 15% u_1 change, and y_3 response for 20% u_1 change roughly follows the same trend with the sum of y_3 response for 5% and 15% u_1 change, and y_2 response for 20% u_2 change roughly follows the same trend with the sum of y_2 response for 5% and 15% u_2 change, and y_3 response for 20% u_2 change roughly follows the same trend with the sum of y_3 response for 5% and 15% u_2 change. Thus, one linear model is enough to represent the original plant when u_1 and u_2 changes 20% respectively at normal load operating point, i.e. there is no need to add any

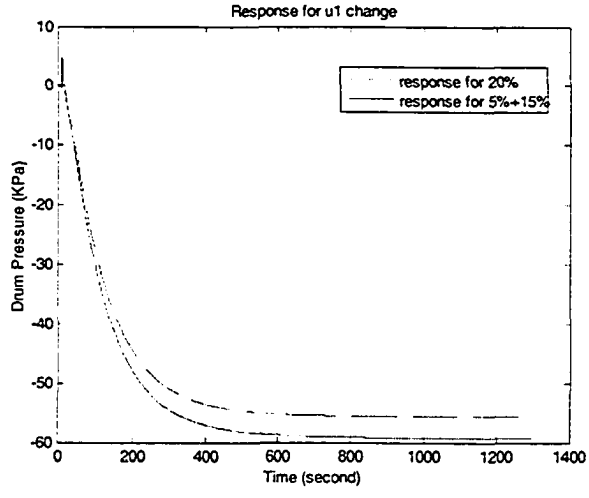

Figure 2-7: y_2 comparison results for additivity at normal load operating point

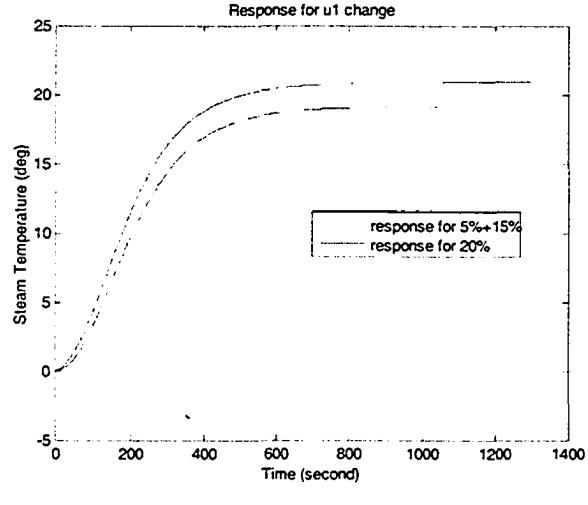

Figure 2-8: y_3 comparison results for additivity at normal load operating point

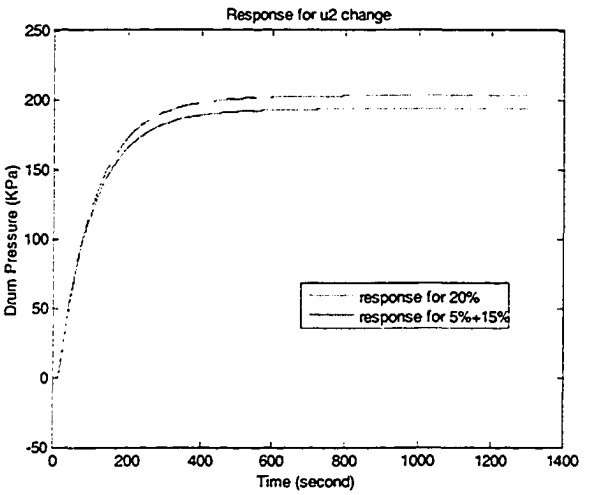

Figure 2-9: y_2 comparison results for additivity at normal load operating point

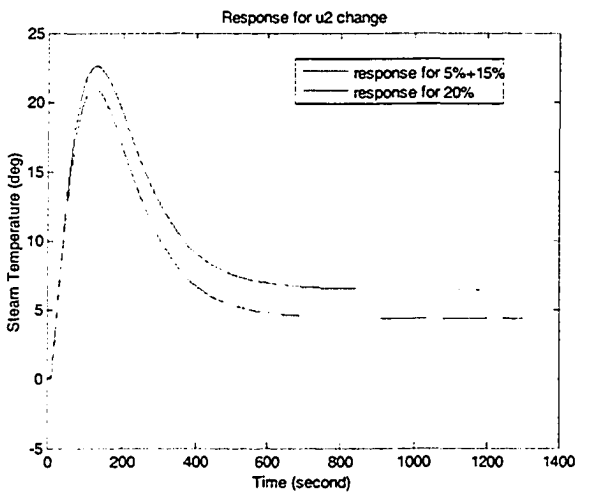

Figure 2-10: y_3 comparison results for additivity at normal load operating point

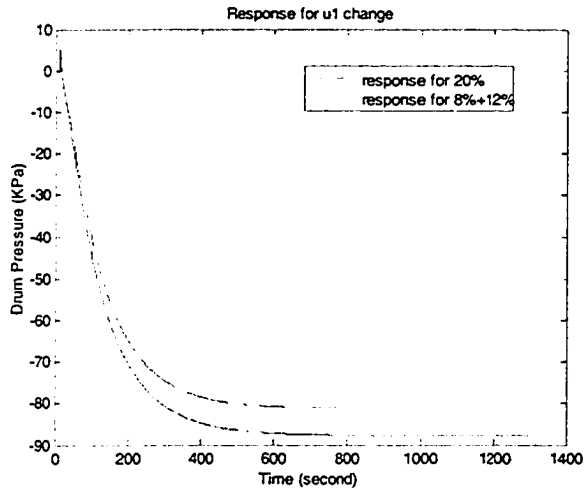

Figure 2-11: y_2 comparison results for additivity at high load operating point

linear model in between normal load operating point and high load operating point.

Since there is no higher load demand than high load whether a linear model can be used to represent the system worked at the high load operating point is checked. 8%, 12% and 20% variation of u_1 are given respectively at high load operating point, and the corresponding outputs of y_2 and y_3 are plotted in Figure 2-11 and Figure 2-12.

Similarly, 8%, 12% and 20% variation of u_2 are given respectively at high load operating point, and the corresponding outputs of y_2 and y_3 are plotted in Figure 2-13 and Figure 2-14.

Figure 2-11-Figure 2-14 show that y_2 response for 20% u_1 change roughly follows the same trend with the sum of y_2 response for 8% and 12% u_1 change, and y_3 response for 20% u_1 change roughly follows the same trend with the sum of y_3 response for 8% and 12% u_1 change, and y_2 response for 20% u_2 change roughly follows the same trend with the sum of y_2 response for 8% and 12% u_2 change, and y_3 response for 20% u_2 change roughly follows the same trend with the sum of y_3 response for 8% and 12% u_2 change. Thus, a linear model can be used to represent the system characteristics

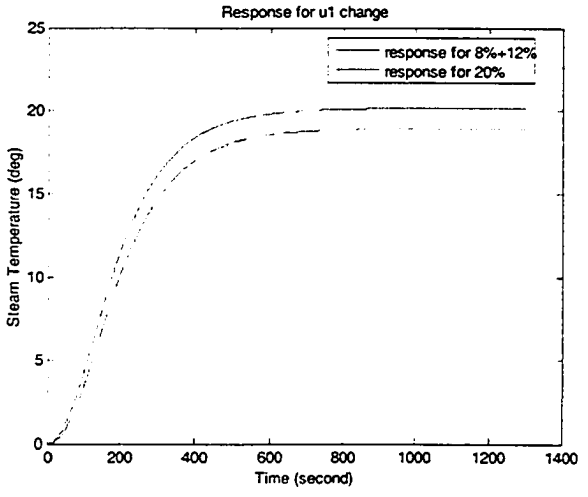

Figure 2-12: y_3 comparison results for additivity at high load operating point

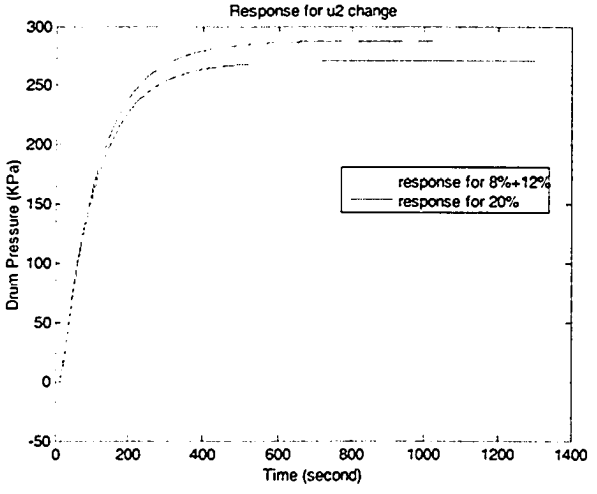

Figure 2-13: y_2 comparison results for additivity at high load operating point

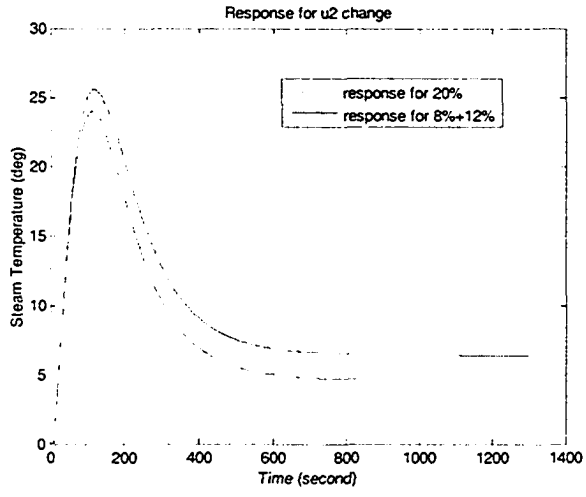

Figure 2-14: y_3 comparison results for additivity at high load operating point

at the high load operating point.

Previous experiment results show that three linear models can represent the entire boiler system, and there exists overlapping area between low load area and normal load area and overlapping area between normal load area and high load area.

2.3.2 Model Identification

As mentioned in previous section the SYNSIM software package describes the plant exactly. However the SYNSIM itself is significantly complex. It is not suitable for controller design. Thus system identification experiments are conducted on SYNSIM at low load operating point, normal load operating point and high load operating point respectively. Then, the Matlab system identification toolbox is used to identify three appropriate LTI models for the three operating points.

Sampling period calculation

The sampling period should be chosen first. Lots of the step input experiment for each channel are conducted. Since the principle for choosing sampling period for different

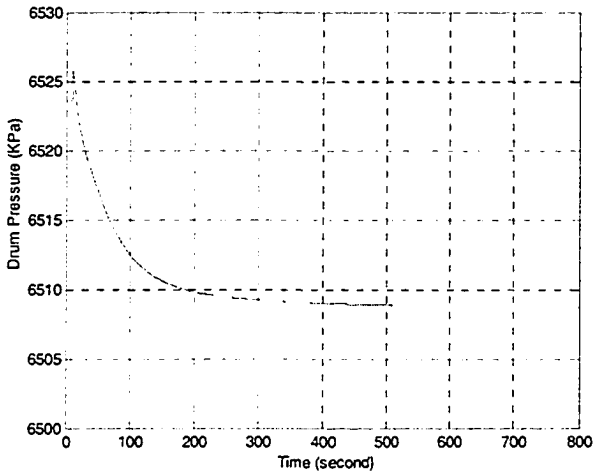

Figure 2-15: Step response of y_2

channels is same only one example is shown here. An experiment around low load operating point is conducted, a step input is excited on u_1 and the step response of y_2 is observed. A step input of u_1 is shown in Figure 2-16, and correspondingly step response of y_2 is shown in Figure 2-15.

"63.2% method" is used to estimate the time constant τ. Figure 2-15 shows that: the initial value $y_0 = 6523.6\ KPa$, the steady state value $y = 6508.7 KPa$, hence $y|_{t=\tau+T_d} = 0.632 * (y - y_0) + y_0 = 0.632 * (6508.7 - 6523.6) + 6523.6 = 6514.2 KPa$, where T_d represents the time delay. And it can be read out from the figure when $t = 76\,s$ the output $y \approx 6514.2\,KPa$. Thus, the time constant $\tau = 76 - 10 = 66\,s$. Since the sampling period is often set to be $(\frac{1}{10} \sim \frac{1}{20})\tau$, sampling period for this channel is chosen as: $T_s = \frac{1}{10}\tau = 6s$.

Input excitation signal design

In the experiment, the random binary sequence (RBS) is used as the input excitation signal. To obtain enough excitation at the low frequency region, the frequency bandwidth of RBS is selected based on the bandwidth of the plant.

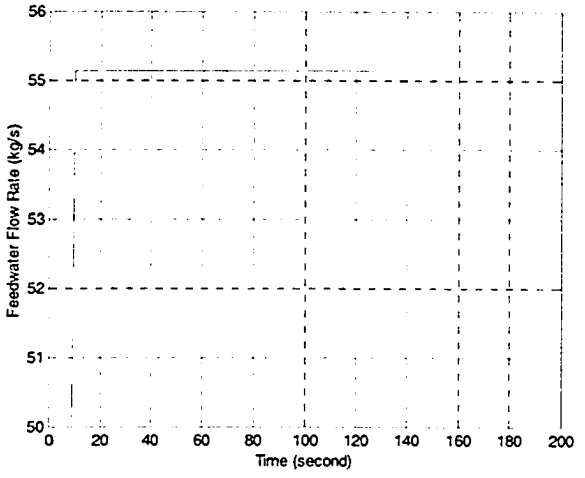

Figure 2-16: Step input of u_1

For the control purpose, only low frequency characteristics of a model is emphasized. Hence, the frequency bandwidth of the RBS should be the cross over frequency of the plant, $\varpi_b = \frac{1}{\tau}$.

In Matlab, the command u=idinput(N, 'rbs',[0,HFR]) is used to generate the RBS, where HFR is to specify the RBS bandwidth as a ratio to the Nyquist frequency ϖ_N.

$$HFR = \frac{\varpi_b}{\varpi_N} = \frac{\varpi_b}{\varpi_s/2} = \frac{1/\tau}{\pi/T_s}$$

Please note that the above calculation is based on the rough estimation of time constant. To ensure the correct bandwidth of the excitation, several RBS are produced using the parameter around calculated HFR. According to the different output results the best HFR that can lead to the enough excitation is chosen.

Model of the utility boiler system

Input-output data are collected from the SYNSIM. First, the time delay for each channel is analyzed. The Matlab command "impulse" is used to plot the impulse figure for the data, and the delay can be roughly read out from the plot, and time

delays were found to be insignificant and were neglected. ARX model, ARMAX model, OE model and BJ model are tested sequentially, and suitable models for different operating points are obtained using trial and error method. The model is defined as follows,

$$G = \begin{bmatrix} G_{11} & G_{12} & G_{13} \\ G_{21} & G_{22} & G_{23} \\ G_{31} & G_{32} & G_{33} \end{bmatrix}$$

For low load operating point, entries are as follows,

$$G_{11}(q^{-1}) = \frac{-0.0003242q^{-1} + 0.0003797q^{-2}}{1 - 1.402q^{-1} + 0.4017q^{-2}}$$

$$G_{12}(q^{-1}) = \frac{0.003145q^{-1} - 0.003181q^{-2}}{1 - 1.976q^{-1} + 0.9758q^{-2}}$$

$$G_{13}(q^{-1}) = 0$$

$$G_{21}(q^{-1}) = \frac{-0.04403q^{-1} + 0.04393q^{-2}}{1 - 1.981q^{-1} + 0.9811q^{-2}}$$

$$G_{22}(q^{-1}) = \frac{1.262q^{-1} - 0.986q^{-2}}{1 - 1.905q^{-1} + 0.9066q^{-2}}$$

$$G_{23}(q^{-1}) = \frac{1.059q^{-1} - 0.9835q^{-2}}{1 - 1.567q^{-1} + 0.5768q^{-2}}$$

$$G_{31}(q^{-1}) = \frac{-0.0006542q^{-1} + 0.0009018q^{-2}}{1 - 1.4q^{-1} + 0.08017q^{-2} + 0.07312q^{-3} + 0.2467q^{-4}}$$

$$G_{32}(q^{-1}) = \frac{0.4301q^{-1} - 1.277q^{-2} + 1.264q^{-3} - 0.4171q^{-4}}{1 - 3.967q^{-1} + 5.901q^{-2} - 3.901q^{-3} + 0.9673q^{-4}}$$

$$G_{33}(q^{-1}) = \frac{0.5584q^{-1} - 0.6976q^{-2}}{1 - 1.507q^{-1} + 0.5134q^{-2}}$$

The above discrete model is converted to continuous model. The entries of the continuous model are as follows,

$$G_{11}(s) = \frac{-0.0005429s + 8.473e - 005}{s^2 + 0.9122s + 9.121e - 005}$$

$$G_{12}(s) = \frac{0.003202s - 3.632e - 005}{s^2 + 0.02458s + 2.448e - 006}$$

$$G_{13}(s) = 0$$

$$G_{21}(s) = \frac{-0.0444s - 0.000103}{s^2 + 0.01909s + 3.369e - 005}$$

$$G_{22}(s) = \frac{1.178s + 0.2894}{s^2 + 0.09808s + 0.001426}$$

$$G_{23}(s) = \frac{1.326s + 0.09864}{s^2 + 0.5502s + 0.01301}$$

$$G_{31}(s) = \frac{-0.0007387s^3 - 0.001744s^2 - 0.001646s + 0.0007188}{s^4 + 1.4s^3 + 5.298s^2 + 0.09806s + 0.0005209}$$

$$G_{32}(s) = \frac{0.4307s^3 + 0.0132s^2 + 2.552e - 006s + 4.031e - 009}{s^4 + 0.03329s^3 + 0.0004684s^2 + 1.736e - 006s + 5.618e - 011}$$

$$G_{33}(s) = \frac{0.8723s - 0.1909}{s^2 + 0.6667s + 0.008722}$$

For normal load operating point, entries are as follows,

$$G_{11}(q^{-1}) = \frac{-0.0002004q^{-1} + 0.0004923q^{-2} - 0.0003539q^{-3} + 6.203e-005q^{-4}}{1 - 2.583q^{-1} + 2.089q^{-2} - 0.4299q^{-3} - 0.07634q^{-4}}$$

$$G_{12}(q^{-1}) = \frac{0.002377q^{-1} - 0.002395q^{-2}}{1 - 1.987q^{-1} + 0.987q^{-2}}$$

$$G_{13}(q^{-1}) = 0$$

$$G_{21}(q^{-1}) = \frac{-0.2217q^{-1} + 0.01216q^{-2}}{1 - 1.268q^{-1} + 0.3206q^{-2}}$$

$$G_{22}(q^{-1}) = \frac{3.573q^{-1} + 3.571q^{-2}}{1 + 0.01339q^{-1} - 0.9854q^{-2}}$$

$$G_{23}(q^{-1}) = \frac{1.182q^{-1} - 0.9612q^{-2}}{1 - 1.372q^{-1} + 0.3972q^{-2}}$$

$$G_{31}(q^{-1}) = \frac{0.01992q^{-1} + 0.006611q^{-2}}{1 - 1.716q^{-1} + 0.7432q^{-2}}$$

$$G_{32}(q^{-1}) = \frac{0.5722q^{-1} - 0.572q^{-2}}{1 - 1.982q^{-1} + 0.9817q^{-2}}$$

$$G_{33}(q^{-1}) = \frac{0.4877q^{-1} - 3.601q^{-2}}{1 - 0.07837q^{-1} - 0.7163q^{-2}}$$

The above discrete model is converted to continuous model. The entries of the continuous model are as follows.

$$G_{11}(s) = \frac{-0.0003421s^3 - 0.0003268s^2 + 6.997e-005s + 4.794e-009}{s^4 + 2.573s^3 + 0.8097s^2 + 1.619e-005s + 8.096e-011}$$

$$G_{12}(s) = \frac{0.002402s - 1.818e-005}{s^2 + 0.01291s + 1.29e-007}$$

$$G_{13}(s) = 0$$

$$G_{21}(s) = \frac{-0.01655s - 0.003535}{s^2 + 0.1138s + 0.0008854}$$

$$G_{22}(s) = \frac{3.599s + 0.002229}{s^2 + 0.01473s + 8.739e-006}$$

$$G_{23}(s) = \frac{0.542s + 0.03762}{s^2 + 0.3078s + 0.00437}$$

$$G_{31}(s) = \frac{0.0003485s + 7.687e-005}{s^2 + 0.01484s + 7.753e-005}$$

$$G_{32}(s) = \frac{0.5774s + 0.000182}{s^2 + 0.0185s + 0.0001025}$$

$$G_{33}(s) = \frac{-0.2439s - 0.007951}{s^2 + 0.04767s + 0.0005245}$$

For high load operating point, entries are as follows,

$$G_{11}(q^{-1}) = \frac{-0.0002384q^{-1} + 0.000503q^{-2} - 0.0002637q^{-3}}{1 - 2.21q^{-1} + 1.43q^{-2} - 0.2192q^{-3}}$$

$$G_{12}(q^{-1}) = \frac{0.002236q^{-1} - 0.00226q^{-2}}{1 - 1.984q^{-1} + 0.9844q^{-2}}$$

$$G_{13}(q^{-1}) = 0$$

$$G_{21}(q^{-1}) = \frac{-0.4032q^{-1} + 0.403q^{-2}}{1 - 1.917q^{-1} + 0.9173q^{-2}}$$

$$G_{22}(q^{-1}) = \frac{31.67q^{-1} - 29.17q^{-2}}{1 - 1.81q^{-1} + 0.8183q^{-2}}$$

$$G_{23}(q^{-1}) = \frac{5.384q^{-1} - 3.614q^{-2}}{1 - 0.4035q^{-1} - 0.4492q^{-2}}$$

$$G_{31}(q^{-1}) = \frac{0.01827q^{-1} - 0.002426q^{-2} + 0.002805q^{-3}}{1 - 2.143q^{-1} + 1.517q^{-2} - 0.3553q^{-3}}$$

$$G_{32}(q^{-1}) = \frac{12.34q^{-1} - 12.23q^{-2}}{1 - 1.606q^{-1} + 0.6471q^{-2}}$$

$$G_{33}(q^{-1}) = \frac{3.336q^{-1} - 4.154q^{-2}}{1 - 0.1189q^{-1} - 0.8157q^{-2}}$$

The above discrete model is converted to continuous model. The entries of the continuous model are as follows,

$$G_{11}(s) = \frac{-0.0004957s^2 + 4.904e - 005s + 1.591e - 006}{s^3 + 1.518s^2 + 0.01734s + 1.732e - 007}$$

$$G_{12}(s) = \frac{0.002266s - 2.362e - 005}{s^2 + 0.01569s + 7.593e - 007}$$

$$G_{13}(s) = 0$$

$$G_{21}(s) = \frac{-0.04208s - 1.69e - 006}{s^2 + 0.008631s + 3.226e - 007}$$

$$G_{22}(s) = \frac{3.358s + 0.02761}{s^2 + 0.02005s + 9.29e - 005}$$

$$G_{23}(s) = \frac{0.3781s + 0.01354}{s^2 + 0.1s + 0.001127}$$

$$G_{31}(s) = \frac{0.0005243s^2 + 5.723e-005s + 3.845e-006}{s^3 + 0.05174s^2 + 0.0008293s + 3.917e-006}$$

$$G_{32}(s) = \frac{0.7635s + 0.0003458}{s^2 + 0.02176s + 0.0001266}$$

$$G_{33}(s) = \frac{-0.08858s - 0.01893}{s^2 + 0.1019s + 0.001514}$$

Modern controller design methods produce order of controllers at least equal to that of the plant and usually higher because of the inclusion of weights [20]. Hence, if the order of the plant is too high the corresponding controller law will be too complex, and it is very difficult or impossible to realize a complex controller in practical application. In order to obtain a simple control law models are simplified . Here different model reduction technique are used, i.e. balanced truncation, balanced residualization and optimal Hankel norm approximation, according to model approximation result the most suitable model reduction technique is used.

The final reduced order LTI model for the low load operating point is shown in (2.1).

$$G = \begin{bmatrix} \frac{-0.0005429s+8.473e-005}{s^2+0.9122s+9.121e-005} & \frac{0.003202s-3.632e-005}{s^2+0.02458s+2.448e-006} & 0 \\ \frac{-0.0444s-0.000103}{s^2+0.01909s+3.369e-005} & \frac{1.178s+0.2894}{s^2+0.09808s+0.001426} & \frac{1.326s+0.09864}{s^2+0.5502s+0.01301} \\ \frac{-0.0003628s+0.0001367}{s^2+0.01862s+9.906e-005} & \frac{0.4952s^2+0.0004161s+1.846e-007}{s^3+0.01336s^2+9.123e-005s+2.462e-009} & \frac{0.8723s-0.1909}{s^2+0.6667s+0.008722} \end{bmatrix} \quad (2.1)$$

In order to validate the final reduced order model the same step input is given to above model and the SYNSIM simulation package, and then the output results are compared. The model validation results are shown in Figure 2-17, Figure 2-18

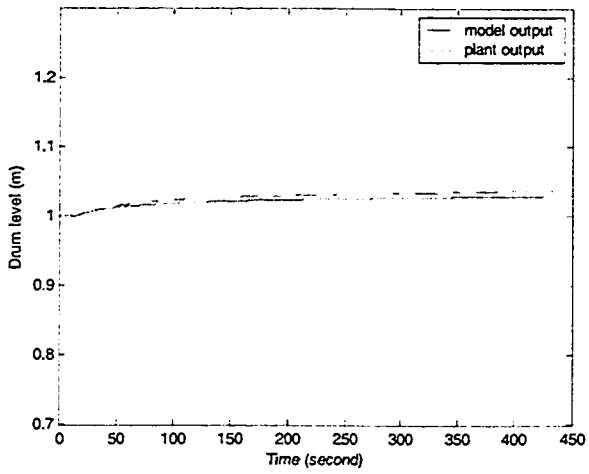

Figure 2-17: Validation result for y_1

and Figure 2-19. In these figures solid line represents the plant step response and dash-dot line represents the model step response respectively.

The validation results show that the transit response of the model and the plant math very well, there exist little difference at the steady state value. In general the model can represent the system very well around the low load operating point.

The final reduced order LTI model for the normal load operating point is shown in (2.2).

$$\begin{bmatrix} \frac{-0.0003421s^3-0.0003268s^2+6.997e-005s+4.794e-009}{s^4+2.573s^3+0.8097s^2+1.619e-005s+8.096e-011} & \frac{0.002402s-1.818e-005}{s^2+0.01291s+1.29e-007} & 0 \\ \frac{-0.01655s-0.003535}{s^2+0.1138s+0.0008854} & \frac{3.599s+0.002229}{s^2+0.01473s+8.739e-006} & \frac{0.542s+0.03762}{s^2+0.3078s+0.00437} \\ \frac{0.0003485s+7.687e-005}{s^2+0.01484s+7.753e-005} & \frac{0.5774s+0.000182}{s^2+0.0185s+0.0001025} & \frac{-0.2439s-0.007951}{s^2+0.04767s+0.0005245} \end{bmatrix} \tag{2.2}$$

Similarly, Figure 2-20, Figure 2-21 and Figure 2-22 show the validation results for model (2.2).

The validation results show that the transit response of the model and the plant math very well, there exist difference at the steady state value, especially for y_1, but

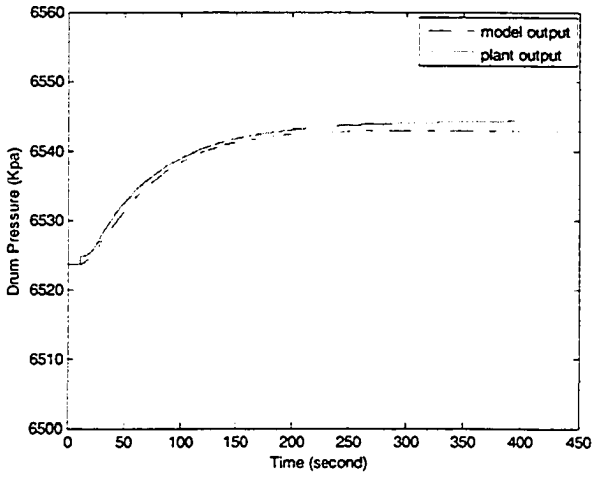

Figure 2-18: Validation result for y_2

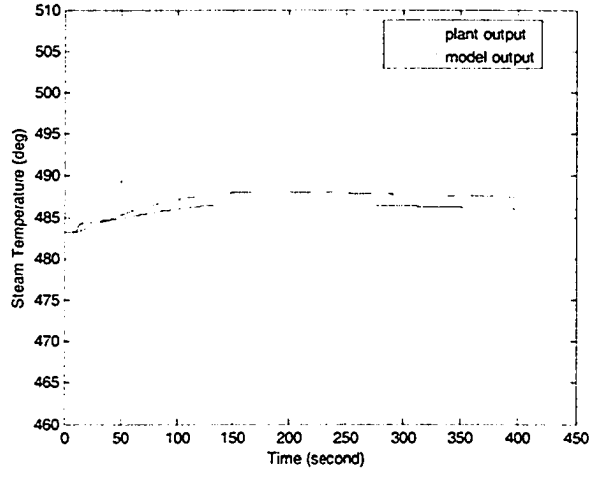

Figure 2-19: Validation result for y_3

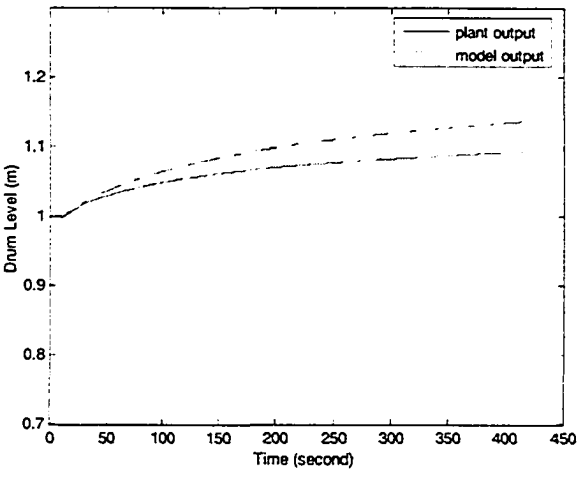

Figure 2-20: Validation result for y_1

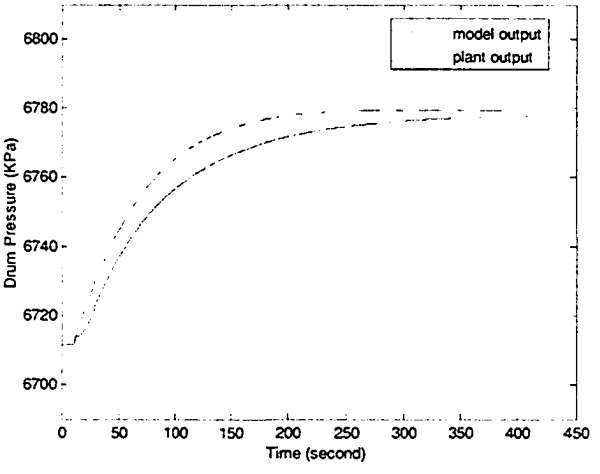

Figure 2-21: Validation result for y_2

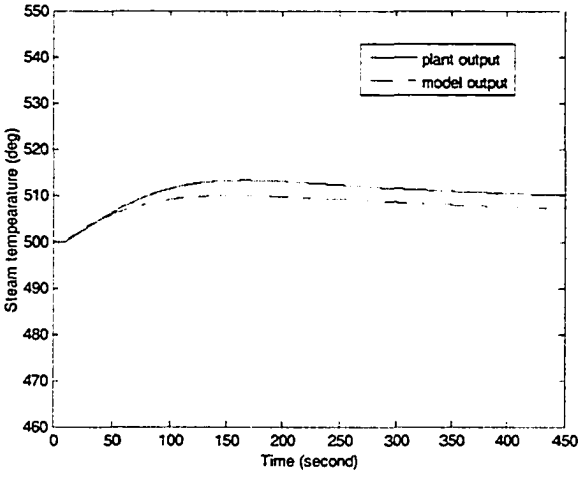

Figure 2-22: Validation result for y_3

for y_1 the trend of the model and the plant are the same. Thus, the model can represent the system very well around the normal load operating point.

The final reduced order LTI model for the high load operating point is shown in (2.3).

$$G = \begin{bmatrix} \frac{-0.0004957s^2+4.904e-005s+1.591e-006}{s^3+1.518s^2+0.01734s+1.732e-007} & \frac{0.002266s-2.362e-005}{s^2+0.01569s+7.593e-007} & 0 \\ \frac{-0.04208s-1.69e-006}{s^2+0.008631s+3.226e-007} & \frac{3.358s+0.02761}{s^2+0.02005s+9.29e-005} & \frac{0.3781s+0.01354}{s^2+0.1s+0.001127} \\ \frac{0.0005243s^2+5.723e-005s+3.845e-006}{s^3+0.05174s^2+0.0008293s+3.917e-006} & \frac{0.7635s+0.0003458}{s^2+0.02176s+0.0001266} & \frac{-0.08858s-0.01893}{s^2+0.1019s+0.001514} \end{bmatrix} \quad (2.3)$$

Figure 2-23, Figure 2-24 and Figure 2-25 show the validation results for model (2.3).

The validation results show that the model represents the plant very well around the high load operating point.

As described in previous part the utility boiler system can be described by three linear models, now three suitable linear models around low load operating point and normal load operating point and high load operating point are obtained respectively.

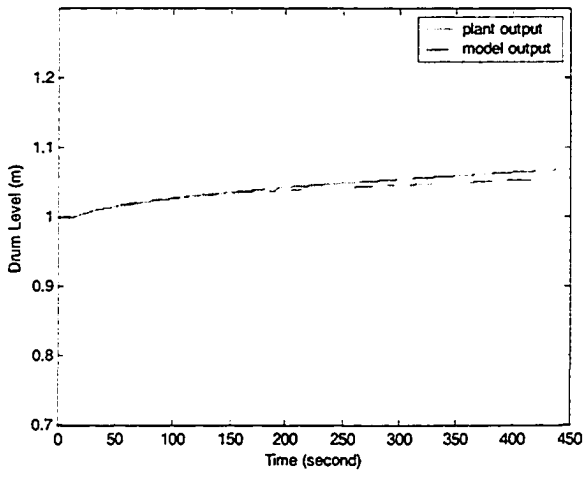

Figure 2-23: Validation result for y_1

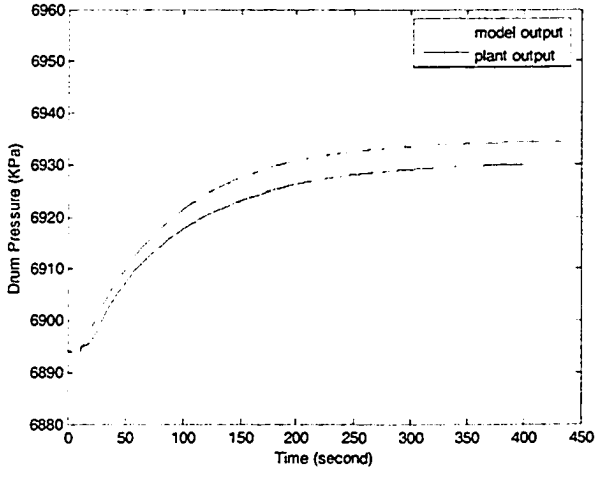

Figure 2-24: Validation result for y_2

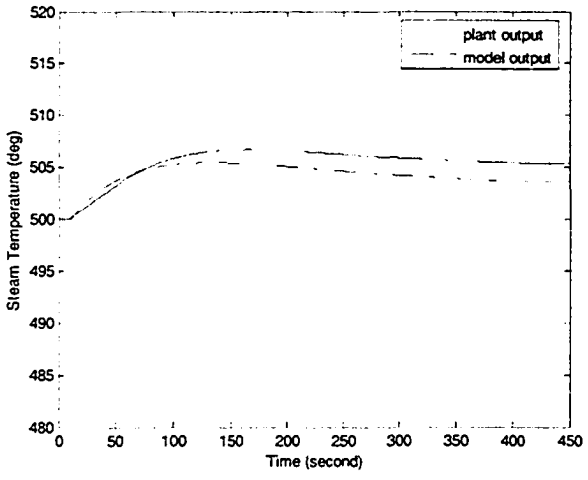

Figure 2-25: Validation result for y_3

Then, the sound linear controller design theory can be employed to design multiple controllers.

Chapter 3

Multiple controller design

3.1 H_∞ optimal control

In order to design a H_∞ optimal controller a general control configuration should be formulated first. Figure 3-1 shows the general control configuration [20].

In this general control configuration figure P is the generalized plant, K is the generalized controller, w represents exogenous inputs, u represents control signals, z represents exogenous outputs and v represents sensed outputs.

Normally the generalized plant P is defined as,

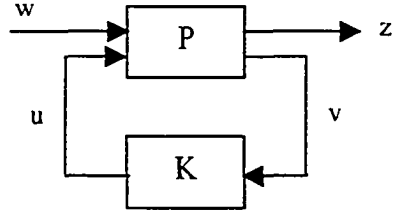

Figure 3-1: General control configuration.

$$P = \left[\begin{array}{c|cc} A & B_1 & B_2 \\ \hline C_1 & D_{11} & D_{12} \\ C_2 & D_{21} & D_{22} \end{array}\right] \tag{3.1}$$

According to Figure 3-1 it is clearly that,

$$\begin{bmatrix} z \\ v \end{bmatrix} = P \begin{bmatrix} w \\ u \end{bmatrix} = \begin{bmatrix} P_{11} & P_{12} \\ P_{21} & P_{22} \end{bmatrix} \begin{bmatrix} w \\ u \end{bmatrix} \tag{3.2}$$

$$u = Kv \tag{3.3}$$

The closed-loop transfer function from w to z is given by the following linear fractional transformation,

$$z = F_l(P, K)w \tag{3.4}$$

where,

$$F_l(P, K) = P_{11} + P_{12}K(I - P_{22}K)^{-1}P_{21} \tag{3.5}$$

The standard H_∞ optimal control problem is to find all stabilizing controllers K which minimize $\|F_l(P, K)\|_\infty$. At frequency domain $\|F_l(P, K)\|_\infty$ is defined as follows,

$$\|F_l(P, K)\|_\infty = \max_w \overline{\sigma}(F_l(P, K)(jw)) \tag{3.6}$$

Correspondingly $\|F_l(P, K)\|_\infty$ can be defined at time domain as follows,

$$\|F_l(P, K)\|_\infty = \max_{w(t)\neq 0} \frac{\|z(t)\|_2}{\|w(t)\|_2} \tag{3.7}$$

where, $\|z(t)\|_2$ and $\|w(t)\|_2$ are the 2-norm of the corresponding vector signal. Following assumptions are made in H_∞ optimal control problems,

1. (A, B_2) is stabilizable and (C_2, A) is detectable.

2. D_{12} and D_{21} have full rank.

3. $\begin{bmatrix} A - j\varpi I & B_2 \\ C_1 & D_{12} \end{bmatrix}$ has full column rank for all ϖ.

4. $\begin{bmatrix} A - j\varpi I & B_1 \\ C_2 & D_{21} \end{bmatrix}$ has full row rank for all ϖ.

3.2 Controller design for each operating point

3.2.1 Model scaling

For the boiler system the scaling is a must due to large range of the magnitude of different channels. Before designing the controller, a scaling of the plant was implemented. According to reference [20] following formula is used to obtain the scaled model:

$$G\_s = D_y^{-1} G D_u \tag{3.8}$$

where,

G_s represents the scaled model, G represents the original model, D_y is diagonal scaling matrix in which each diagonal entry is the largest output change, D_u is diagonal scaling matrix in which each diagonal entry is the largest allowed input change.

Experiments are conducted on model (2.1), (2.2) and (2.3) respectively to obtain D_y with given D_u.

For the low load operating point ,

$$D_y = \begin{bmatrix} 1 & & \\ & 178.6 & \\ & & 27.14 \end{bmatrix}, \; D_u = \begin{bmatrix} 18.24 & & \\ & 1.05 & \\ & & 0.58 \end{bmatrix}$$

Thus, the scaled model of the low load operating point is as follows,

$$G\_s = \begin{bmatrix} \frac{-0.009902s+0.001545}{s^2+0.9122s+9.121e-005} & \frac{0.003362s-3.813e-005}{s^2+0.02458s+2.448e-006} & 0 \\ \frac{-0.004535s-1.052e-005}{s^2+0.01909s+3.369e-005} & \frac{0.006924s+0.001701}{s^2+0.09808s+0.001426} & \frac{0.004307s+0.0003203}{s^2+0.5502s+0.01301} \\ \frac{-0.0002438s+9.188e-005}{s^2+0.01862s+9.906e-005} & \frac{0.01916s^2+1.61e-005s+7.142e-009}{s^3+0.01336s^2+9.123e-005s+2.462e-009} & \frac{0.01864s-0.004079}{s^2+0.6667s+0.008722} \end{bmatrix} \tag{3.9}$$

For the normal load operating point,

$$D_y = \begin{bmatrix} 1 & & \\ & 173.1 & \\ & & 7 \end{bmatrix}, D_u = \begin{bmatrix} 13.38 & & \\ & 0.84 & \\ & & 1.26 \end{bmatrix}$$

Thus, the scaled model of the normal load operating point is as follows,

$$\begin{bmatrix} \frac{-0.004577s^3-0.004373s^2+0.0009361s+6.415e-008}{s^4+2.573s^3+0.8097s^2+1.619e-005s+8.096e-011} & \frac{0.002018s-1.527e-005}{s^2+0.01291s+1.29e-007} & 0 \\ \frac{-0.00128s-0.0002732}{s^2+0.1138s+0.0008854} & \frac{0.01746s+1.082e-005}{s^2+0.01473s+8.739e-006} & \frac{0.003945s+0.0002738}{s^2+0.3078s+0.00437} \\ \frac{0.0006662s+0.0001469}{s^2+0.01484s+7.753e-005} & \frac{0.06929s+2.184e-005}{s^2+0.0185s+0.0001025} & \frac{-0.0439s-0.001431}{s^2+0.04767s+0.0005245} \end{bmatrix} \tag{3.10}$$

For the high load operating point,

$$D_y = \begin{bmatrix} 0.38 & & \\ & 95.24 & \\ & & 12.04 \end{bmatrix}, D_u = \begin{bmatrix} 8.17 & & \\ & 0.45 & \\ & & 0.18 \end{bmatrix}$$

Thus, the scaled model of the high load operating point is as follows,

$$G\_s = \begin{bmatrix} \frac{-0.01063s^2+0.001052s+3.414e-005}{s^3+1.518s^2+0.01734s+1.732e-007} & \frac{0.002664s-2.778e-005}{s^2+0.01569s+7.593e-007} & 0 \\ \frac{-0.003611s-1.45e-007}{s^2+0.008631s+3.226e-007} & \frac{0.0158s+0.0001299}{s^2+0.02005s+9.29e-005} & \frac{0.0007305s+2.616e-005}{s^2+0.1s+0.001127} \\ \frac{0.0003559s^2+3.885e-005s+2.61e-006}{s^3+0.05174s^2+0.0008293s+3.917e-006} & \frac{0.02841s+1.287e-005}{s^2+0.02176s+0.0001266} & \frac{-0.001354s-0.0002893}{s^2+0.1019s+0.001514} \end{bmatrix} \tag{3.11}$$

According to the scaled model the corresponding controller C can be designed.

The final controller is obtained as follows:

$$C_{final} = D_y^{-1} C D_u$$

3.2.2 H_∞ controller design

In this section the method how to design controllers at each operating point is introduced.

The true plant is assumed as follows,

$$G = P + \Delta_p \tag{3.12}$$

where,

P is the LTI model for corresponding operating point, and P can be represented as following:

$$\begin{aligned} \dot{x} &= Ax + Bu \\ y &= Cx + Du \end{aligned} \tag{3.13}$$

Δ_p represents additive model uncertainty associated with the linear time-invariant model G and can be used to account for the difference in the prediction by the model. Notice that this assumption emphasizes that, within the operating region each local model can be assumed to be accurately represented by a linear system. Thus that Δ_p is norm bounded is assumed, i.e. Δ_p satisfies an inequality of the form $|\Delta_p(j\varpi)| \leq l(j\varpi)$. Also, $\Delta_p = \Delta W_2$, where $\|\Delta\|_\infty < 1$.

A feedback closed-loop system is formed which is shown in Figure 3-2. In this figure C represents controller, P represents the plant, Δ is the uncertainty, W_1 and W_2 are weighting functions.

The closed-loop system can be cast into the $M - \Delta$ form, which is shown in Figure

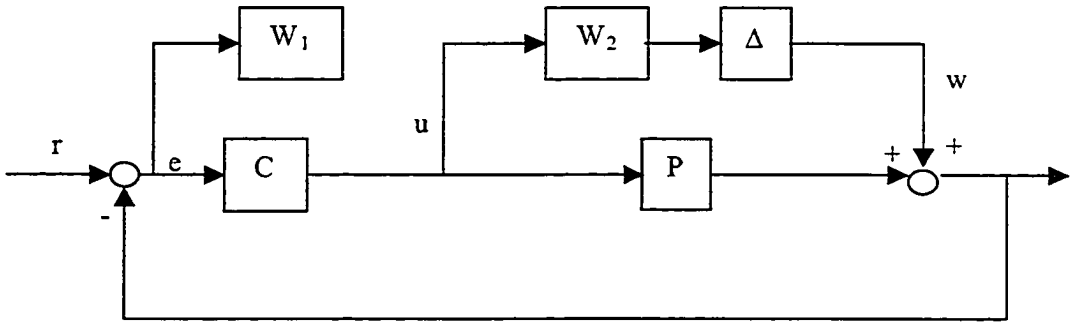

Figure 3-2: Closed-loop system

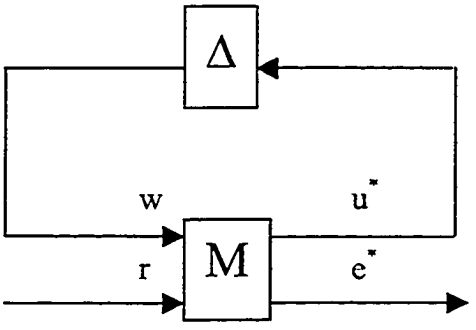

Figure 3-3: $M - \Delta$ form of the closed-loop system

3-3. Where,

$$M = \begin{bmatrix} -W_2CS & W_2CS \\ -W_1S & W_1S \end{bmatrix}$$

Where, $S = (I + PC_i)^{-1}$ is the sensitivity function.

The problem to solve is: find a stabilizing controller C such that the H_∞ normal of the M is less than 1 for all Δ, where $\|\Delta\|_\infty < 1$. The controller is obtained by using μ-synthesis and the DK-iteration method. The idea of the DK-iteration method comes from the following inequality,

$$\mu(M) \leq \min \bar{\sigma}(DMD^{-1}) \tag{3.14}$$

Where, D is the block-diagonal matrix.

Thus, DK-iteration method is used to find the controller that minimizes the peak value over frequency of this upper bound,

$$\min_{C}(\min \left\| DMD^{-1} \right\|_{\infty}) \tag{3.15}$$

Reference [20] provides a detailed description of the DK-iteration method.

3.2.3 Weighting

Weight selection is very important because it is directly related with the controller performance. In fact the weighting functions serve as the primary tuning parameter of the controller design.

For performance weighting function W_1 following criteria are obeyed [21]:

1. Steady-state offset less than 0.
2. Closed-loop bandwidth higher than ϖ_B
3. Amplification of high-frequency noise less than a factor M.

Thus, following formula is used to obtain the performance weighting function W_1.

$$W_1 = \frac{s/M + \varpi_B}{s + \varpi_B A} \tag{3.16}$$

After exhaustive trial and error we choose weighting function as follows.

For the low load model W_1 is chosen as follows:

$$W_1 = \begin{bmatrix} \frac{0.2s+0.012}{s+0.0000012} & & \\ & \frac{0.2s+0.0015}{s+0.00000015} & \\ & & \frac{0.2s+0.01}{s+0.000001} \end{bmatrix} \tag{3.17}$$

And W_2 is chosen as follows:

$$W_2 = \begin{bmatrix} \frac{14s}{s+10} & & \\ & \frac{14s+10}{s+15} & \\ & & \frac{14s+0.3}{s+15} \end{bmatrix} \tag{3.18}$$

For the normal load model W_1 is chosen as follows:

$$W_1 = \begin{bmatrix} \frac{0.2s+0.005}{s+0.0000005} & & \\ & \frac{0.2s+0.008}{s+0.0000008} & \\ & & \frac{0.2s+0.02}{s+0.000002} \end{bmatrix} \tag{3.19}$$

And W_2 is chosen as follows:

$$W_2 = \begin{bmatrix} \frac{14s+1}{s+10} & & \\ & \frac{14s+1}{s+15} & \\ & & \frac{14s+0.3}{s+15} \end{bmatrix} \tag{3.20}$$

For the high load model W_1 is chosen as follows:

$$W_1 = \begin{bmatrix} \frac{0.2s+0.01}{s+0.000001} & & \\ & \frac{0.2s+0.01}{s+0.000001} & \\ & & \frac{0.2s+0.01}{s+0.000001} \end{bmatrix} \tag{3.21}$$

And W_2 is chosen as follows:

$$W_2 = \begin{bmatrix} \frac{14s}{s+10} & & \\ & \frac{14s+1}{s+15} & \\ & & \frac{14s+0.3}{s+15} \end{bmatrix} \tag{3.22}$$

3.2.4 Controller reduction

Previous H_∞ controller design algorithm always leads a high order controller. As a result, the low load H_∞ controller has order 35; the normal load H_∞ controller has order 40; the high load H_∞ controller has order 36. It is very difficult to implement

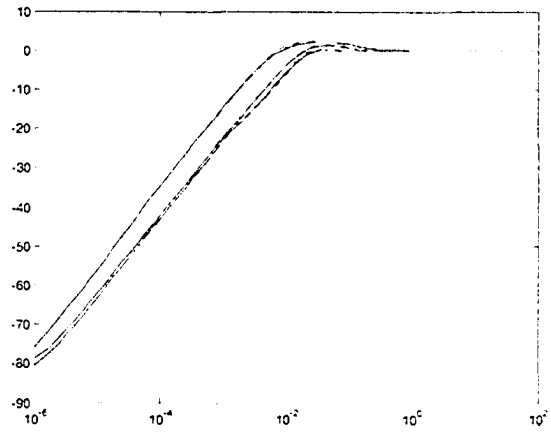

Figure 3-4: Comparison result for the singular values of S for the low load controller

such high order controllers in the real application. Thus, model reduction technique is used again to obtain reduced order controllers. The balanced truncation method is used to reduce the order. The controller reduction objective is to find minimal order controllers which achieve the same control effect as the corresponding full-order controller. Thus, first the reduced order controller is obtained, and then it is realized on the SYNSIM for testing the control effect. Finally, the minimum reduced controller which achieves the similar control effect as the full-order controller is chosen. The singular values of the S for original controllers and corresponding reduced order controller are calculated and compared. Figure 3-4~Figure 3-6 show the comparison results for the low load controller, normal load controller and high load controller. In all of the three figures the solid lines represent the singular values of S for the original controller and the dotted lines represent the singular values of S for the reduced order controller. The results show that the original controllers and the reduced order controllers have similar characteristics.

As a result, the order of reduced low load controller is 13, the order of reduced normal load controller is 7, and the order of reduced high load controller is 9. State

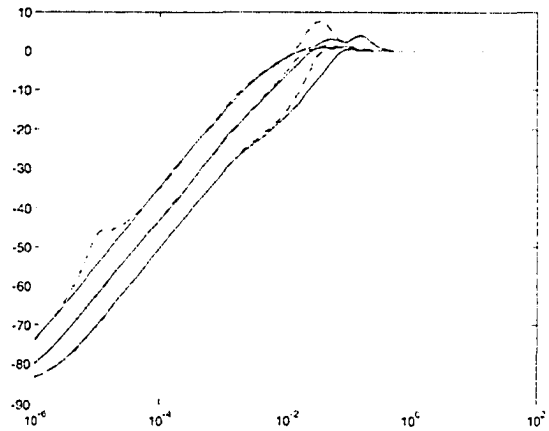

Figure 3-5: Comparison result for the singular values of S for the normal load controller

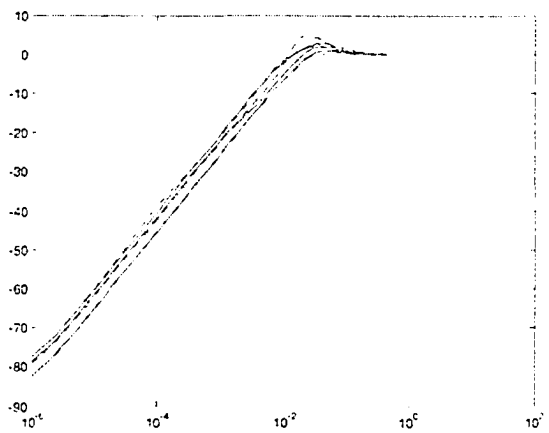

Figure 3-6: Comparison result for the singular values of S for the high load controller

space realizations of the final controllers are in the Appendix.

3.3 Switching algorithm

3.3.1 Observer design

In order to realize controller switching algorithm the system states should be known. Since the system states are immeasurable an observer should be designed. The best way is to design a nonlinear observer. However the nonlinear model of the boiler system is unavailable. Similar as the idea to use multiple model to represent the boiler system different observers are designed around different operating points. i.e. low load observer, normal load observer, and high load observer.

According to [22] the method of designing each observer is as follows.

Consider the n-dimension p-input and q-output state equation,

$$\begin{aligned} \dot{x} &= Ax + Bu \\ y &= Cx \end{aligned} \tag{3.23}$$

Obviously the closed-loop observer is,

$$\dot{\hat{x}} = (A - LC)\hat{x} + Bu + Ly \tag{3.24}$$

The error vector is,

$$e(t) := x(t) - \hat{x}(t) \tag{3.25}$$

Then,

$$\dot{e} = (A - LC)e \tag{3.26}$$

If (A, C) is observable, then all eigenvalues of $(A - LC)$ can be assigned arbitrarily by choosing an L.

For the low load model, the eigenvalues of $(A - LC)$ are chosen as follows,

$-0.4 \pm 0.3i$; $-0.5 \pm 0.4i$; $-0.2 \pm 0.2i$; -0.02; -0.03; $-0.015 \pm 0.005i$; $-0.02 \pm 0.005i$; $-0.01 \pm 0.005i$; $-0.04 \pm 0.01i$.

In order to check whether the observer is good enough experiments are conducted on Matlab Simulink. The model is excited by some inputs, and the states of the model and the estimated states from the observer are measured. Results shows that the low load observer works very well.

For the normal load model, the eigenvalues of $(A - LC)$ are chosen as follows,

-30; -25; -0.01; -0.02; -1.2; -0.1053; -0.0304; -0.1; $-0.0074 \pm 0.0047i$; -1; -1.2; -0.0129; -0.0141; -0.0172; -0.0149.

Similarly, the model states and the observed states are measured. Results show that the normal load observer works very well.

For the high load model, the eigenvalues of $(A - LC)$ are chosen as follows,

-0.09; -0.05; -0.04; -0.04; -0.4; -5; -1; -1; -0.012; -0.02; -0.028; -0.036; -0.044; -0.005; -0.001; -0.0072.

Similarly, the model states and the observed states are measured. Results show that the high load observer works very well.

3.3.2 Controller switching

Previous test results of Section 2.3.1 show that there exists overlapping area among low load model, normal load model and high load model. According to reference [3] the states of each model should be checked to judge whether the states go into the overlapping area of different models. If the states go into the desired overlapping areas the controller switching should occur correspondingly. Thus, the system has a stable motion, and then the system stability is ensured. The architecture of the control system for the boiler system based on the input-output approach is shown in

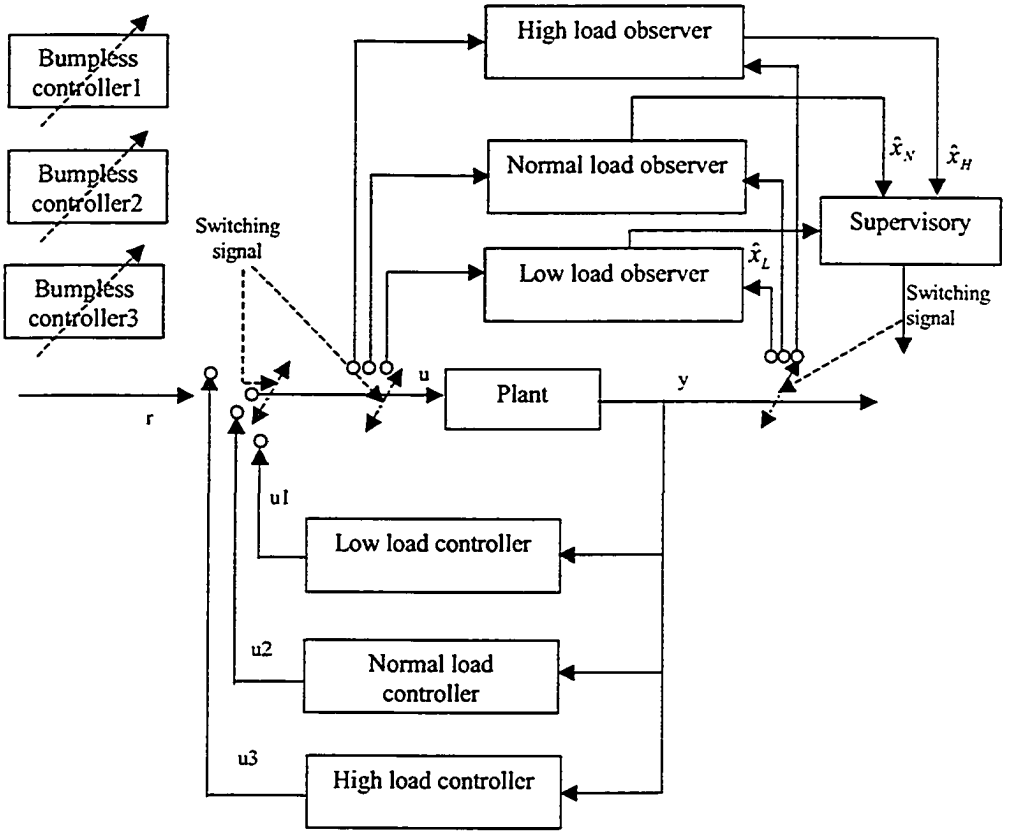

Figure 3-7: Architecture of the control system

Figure 3-7.

The local linear observers and controllers are connected with SYNSIM package, and the results show that part of the system states reach the overlapping area very fast, and other part of them reach the overlapping area slowly. Obviously,transition are dominated by the slow states. Thus, the actual algorithm was implemented using only the "slow" states. The system state values in the overlapping area for the slow system states at different operating points can be obtained by the experiments. The values are shown in Table 3.1. Theoretically, the switching can occur if the system states reach the points in Table 3.1. However, in the practical situation it is difficult to measure just a point considering disturbance. A small region which centers the point is checked. It is considered that the system states have already reached

the corresponding overlapping area when they enter into this region. The following condition is used to decide whether the system states go into the overlapping area:

$$||x - x_s||_2 < 10 \tag{3.27}$$

where x is the observed system states, and x_s is the corresponding system state values which are listed in Table 3.1.

Low load	Normal load	High Load
$x_{2s} = 807$	$x_{5s} = 0$	$x_{4s} = -2930$
$x_{3s} = -4146$	$x_{6s} = 330$	$x_{6s} = 926.7$
$x_{14s} = 14.64$		
$x_{16s} = 42.3$		

Table 3.1: Slow varied system state values

The objective of the switching algorithm is to select an appropriate controller from the three controllers. From the above discussion, it can be seen that the current operating regime and the desired operating regime should be known, and then an appropriate stable motion path could be decided. In order to judge current working operating regime the drum pressure is measured since it varies sufficiently slowly and reflects the effect of nonlinearities on the boiler behavior [19]. The desired set points are used to decide the desired operating regime. Once the current working operating regime and the desired operating regime are known, the corresponding controller action can be easily decided. All possible controller actions are listed in Table 3.2.

Generally, the steps of controller switching algorithm can be described as follows,

Step1: Measure steam pressure of the boiler system to decide current working operating space;

Step2: Decide the desired operating space according to the desired set point;

Step3: Choose corresponding controller action according to Table 3.2;

Step4: First controller is used, if controller switching should be used, the condition of the Equation (3.27) is checked;

Case	Operating regimes change	Controller action
1	Within low load	Use low load controller
2	Within normal load	Use normal load controller
3	Within high load	Use high load controller
4	From low load to normal load	(i) Low load controller (ii) Normal load controller
5	From low load to high load	(i) Low load controller (ii) Normal load controller (iii) High load controller
6	From normal load to high load	(i) Normal load controller (ii) High load controller
7	From high load to normal load	(i) High load controller (ii) Normal load controller
8	From high load to low load	(i) High load controller (ii) Normal load controller (iii) Low load controller
9	From normal load to low load	(i) Normal load controller (ii) Low load controller

Table 3.2: Possible controller action

Step5: If the condition of the Equation (3.27) is not satisfied then go back to Step4;

Step6: If the condition of the Equation (3.27) is satisfied then wait until the dwell time $\tau_D = 10s$ is elapsed. Again check whether the condition of the Equation (3.27) is still satisfied;

Step7: If the condition of the Equation (3.27) is not satisfied then go back to Step4;

Step8: If the condition of the Equation (3.27) is satisfied then switch to the appropriate controller;

Step9: Repeat Step4 - Step8 until the required stable motion is finished;

Step10: Goto Step1.

3.3.3 Controller Initialization

Controller initialization means that no bump occurs in the control signal during transfer among alternative controllers [53]. As shown in [54], the bumpless transfer problem can be considered as a controller design problem, i.e. a new controller should be designed so that the active controller output is mapped to the latent controller output. In [54] the bumpless transfer method among SISO controllers is given. In this thesis the result is extended to the bumpless transfer among MIMO controllers. A one-degree-of-freedom controller is designed to force the latent controller output tracking to the active controller output instead of two-degree-of-freedom controller which is used in [54]. Since there are three different controllers three bumpless controllers should be designed. Here the bumpless controller design for the switch occurring from low load controller to normal load controller is used as an example to show the work principle. Figure 3-8 shows the bumpless transfer diagram. The solid lines in the figure show the active close loop. Once switching signal is activated the normal load controller will take charge of the system and the bumpless controller $C_{bumpless}$ will inactive. Obviously, the bumpless controller $C_{bumpless}$ works only before the switching occurs. Considering the function of the bumpless controller Figure 3-8 can be transformed into Figure 3-9. Clearly, Figure 3-9 shows a typical feedback loop in which $C_{bumpless}$ is a controller and C_{normal} is a controlled plant. Since the plant in this control system is a controller, $C_{bumpless}$ is a controller-controller. Moreover, $C_{bumpless}$ is relatively easy to be designed for the accurate plant model is obtained. Many MIMO controller design techniques can be used to design the controller $C_{bumpless}$. In this thesis H_∞ controller design method is used to design all three bumpless controllers. In order to test the bumpless controller effect the bumpless controllers and multiple local controllers are connected with the SYNSIM package. The results are shown in Figure 3-10 $\sim$ Figure 3-18. Figure 3-10 $\sim$ Figure 3-12 show how bumpless controller1 forces the normal load controller output tracking the low load controller output. Figure 3-13 $\sim$ Figure 3-15 show how bumpless controller2 forces the high load controller

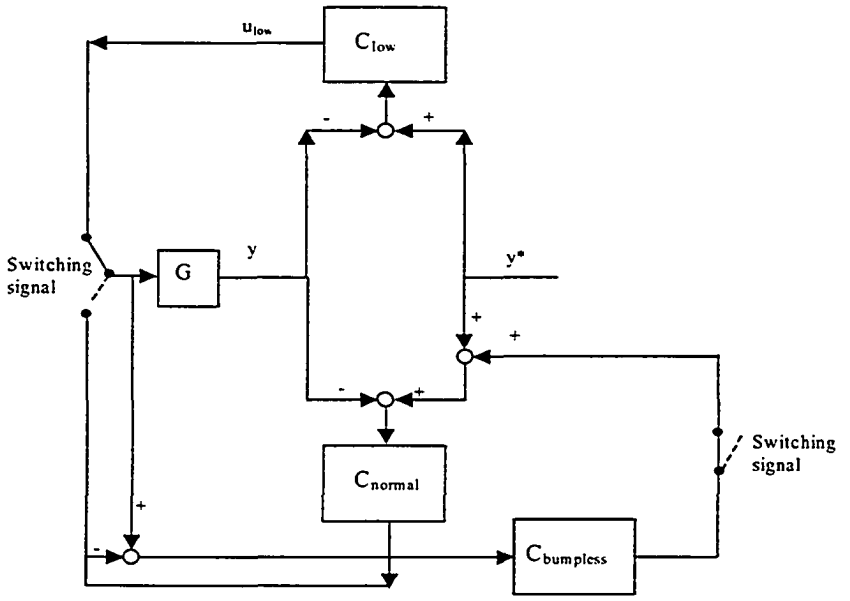

Figure 3-8: Bumpless transfer for switching from low load controller to normal load controller

output tracking the normal load controller output. Figure 3-16 ~ Figure 3-18 show how bumpless controller3 forces the low load controller output tracking normal load controller output. Here, the bumpless controller1 is designed considering normal load controller as the controlled plant. The bumpless controller2 is designed considering high load controller as the controlled plant. The bumpless controller3 is designed considering low load controller as the controlled plant. The simulation results show that all three bumpless controller can achieve the bumpless transfer.

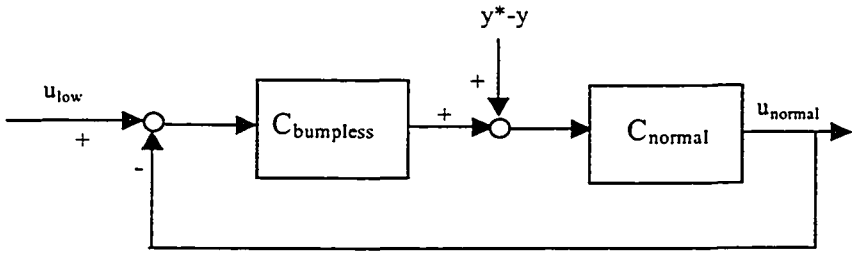

Figure 3-9: Bumpless control loop before the controller switching

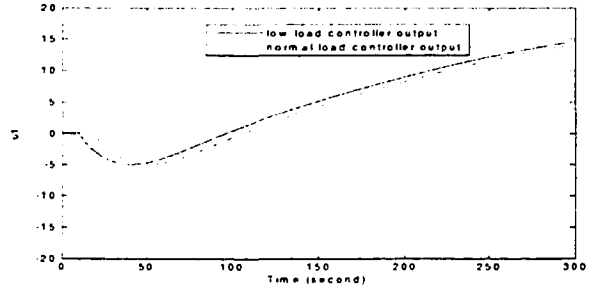

Figure 3-10: u_1 normal load controller output tracks low load controller output

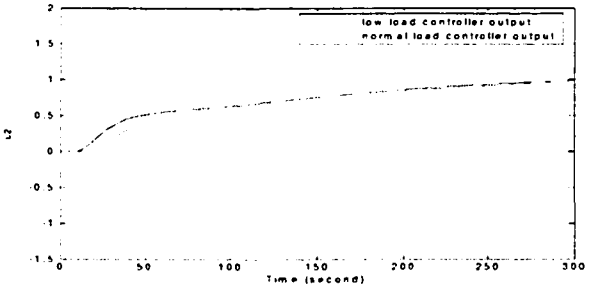

Figure 3-11: u_2 normal load controller output tracks low load controller output

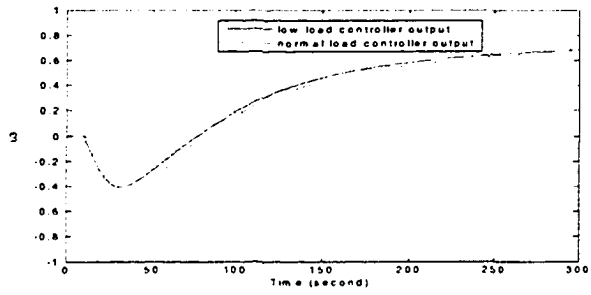

Figure 3-12: u_3 normal load controller output tracks low load controller output

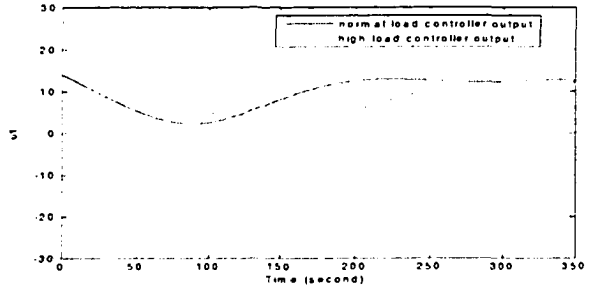

Figure 3-13: u_1 high load controller output tracks normal load controller output

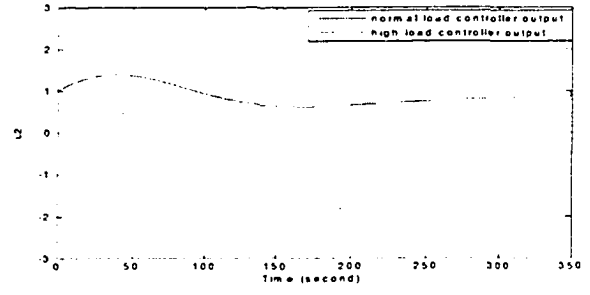

Figure 3-14: u_2 high load controller output tracks normal load controller output

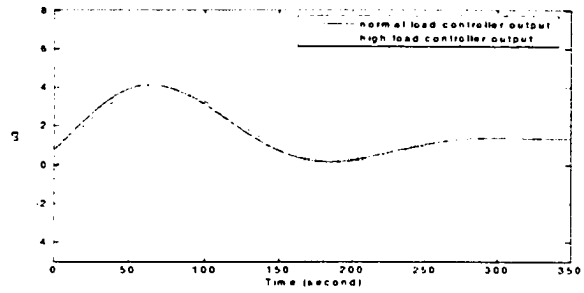

Figure 3-15: u_3 high load controller output tracks normal load controller output

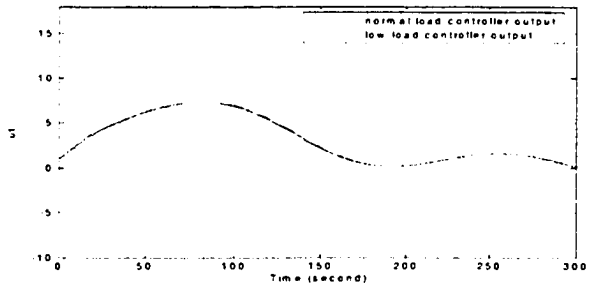

Figure 3-16: u_1 low load controller output tracks normal load controller output

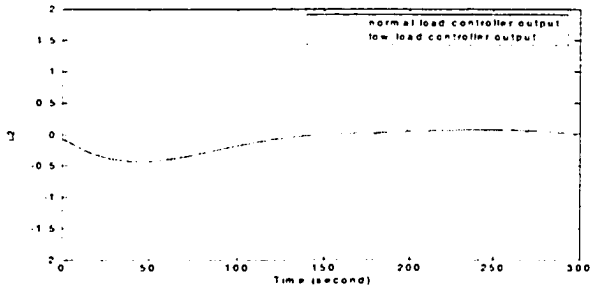

Figure 3-17: u_2 low load controller output tracks normal load controller output

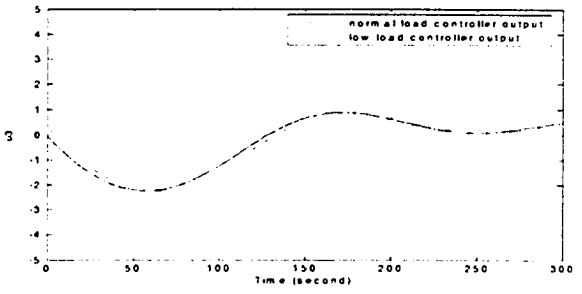

Figure 3-18: u_3 low load controller output tracks normal load controller output

Chapter 4

Simulation results

In order to verify the previous controller design and switching algorithm some experiments are conducted.

First, the three local controllers are connected to the SYNSIM simulation package respectively under three different operating spaces, and controlling effects are evaluated. For the low load operating space following set points are set: drum level is 1 m, drum pressure is 6712 KPa, steam temperature is 500 $°C$; For the normal load operating space following set points are set: drum level is 1 m, drum pressure is 6894 KPa, steam temperature is 500 $°C$; For the high load operating space following set points are set: drum level is 1 m, drum pressure is 7044 KPa, set point of steam temperature is 520 $°C$. Figure 4-1 , Figure 4-2 and Figure 4-3 show the output response at low load operating space, Figure 4-4 , Figure 4-5 and Figure 4-6 show the output response at normal load operating space, Figure 4-7, Figure 4-8 and Figure 4-9 show the output response at high load operating space. The results show that each controller achieve the good performance for the corresponding operating space.

Second, the control effect of the switching algorithm is checked. The most complex situation is that the controlled system goes through all three operating regimes. Hence, the system starting point at low load operating space and the end point at high load operating space are chosen. In this case the controller should switch among

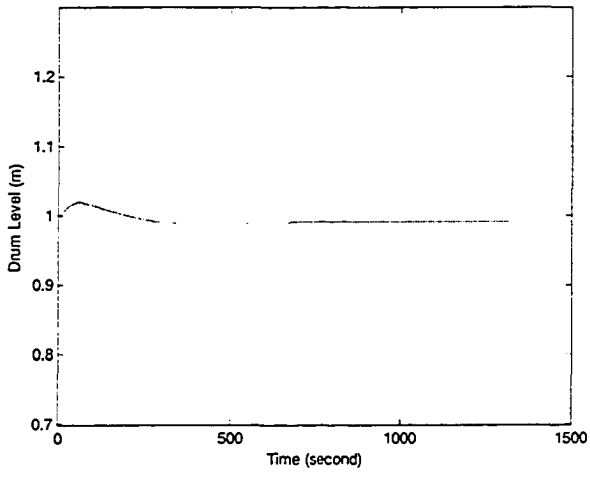

Figure 4-1: y_1 output result at low load operating point

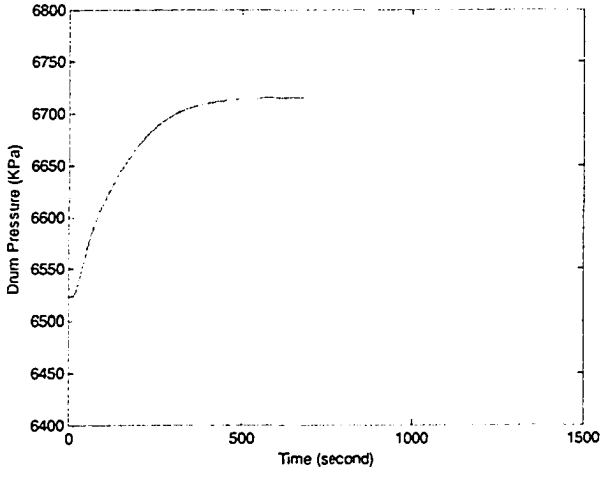

Figure 4-2: y_2 output result at low load operating point

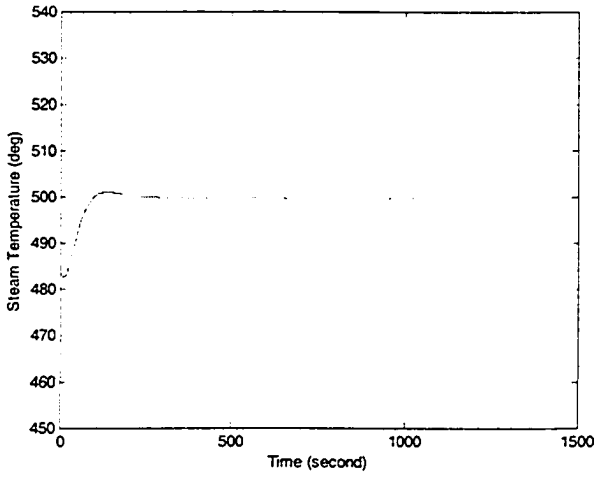

Figure 4-3: y_3 output result at low load operating point

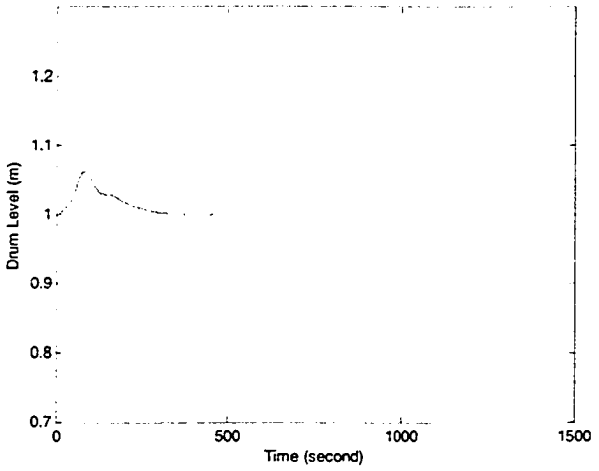

Figure 4-4: y_1 output result at normal load operating point

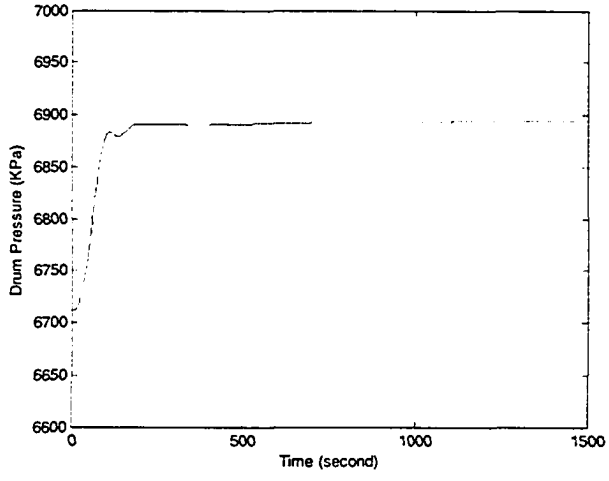

Figure 4-5: y_2 output result at normal load operating point

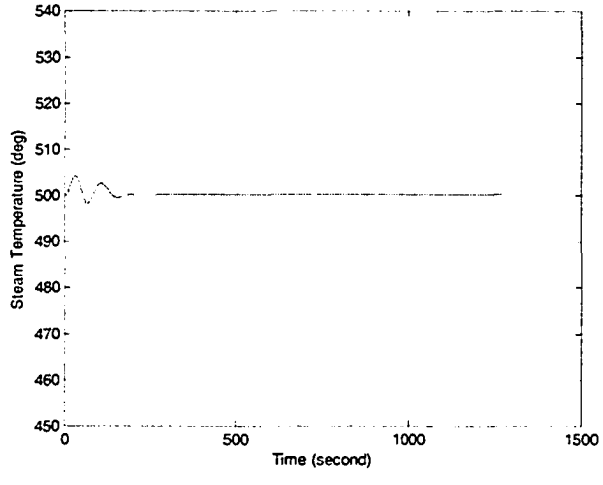

Figure 4-6: y_3 output result at normal load operating point

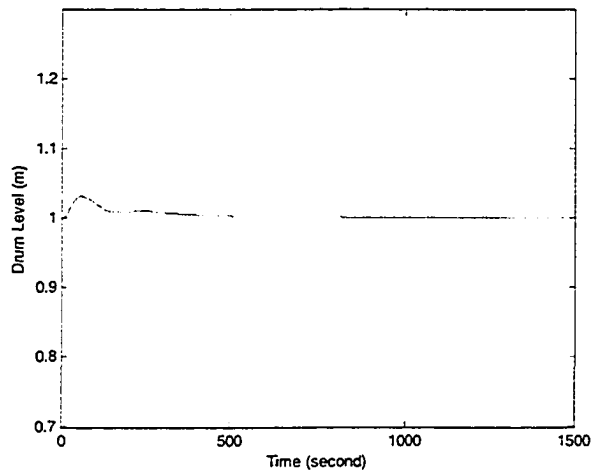

Figure 4-7: y_1 output result at high load operating point

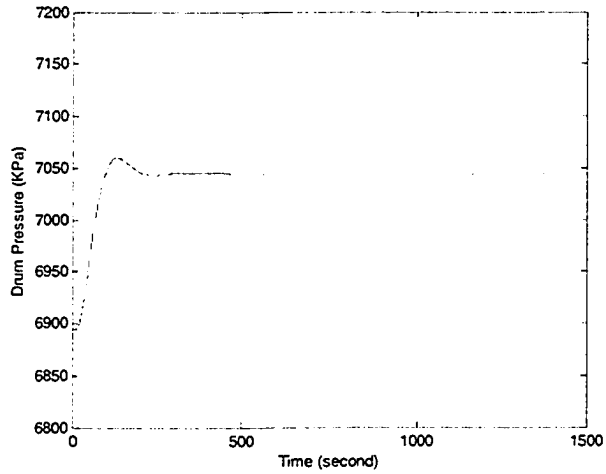

Figure 4-8: y_2 output result at high load operating point

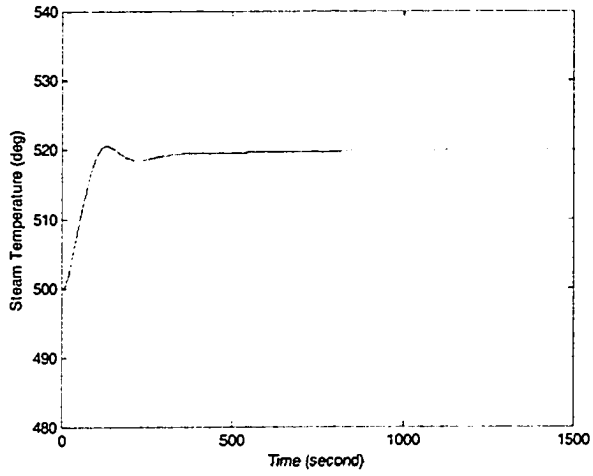

Figure 4-9: y_3 output result at high load operating point

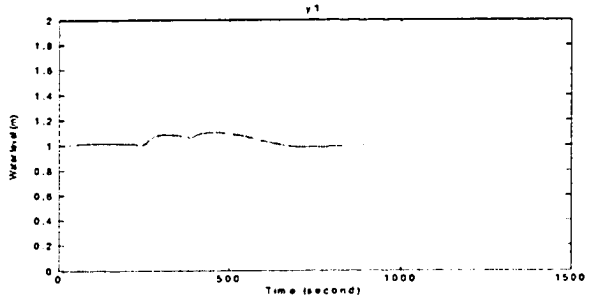

Figure 4-10: y_1 time response

all three controllers. Thus the set points are chosen as follows: Set point of drum level keep unchanged; set point of drum pressure varies from 6523.6 KPa to 7044 KPa; set point of steam temperature varies from 483.19 $°C$ to 520 $°C$. Figure 4-10, Figure 4-11 and Figure 4-12 show the simulation result. Figures show that the boiler system achieves the desired set point very well and at the same time the system stability is maintained.

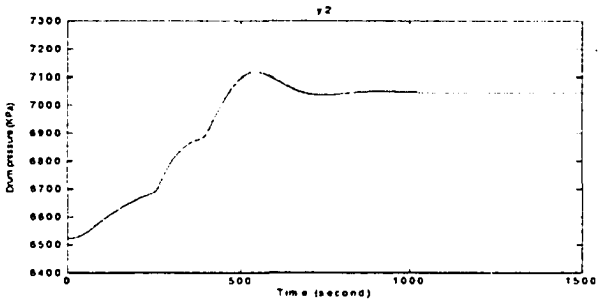

Figure 4-11: y_2 time response

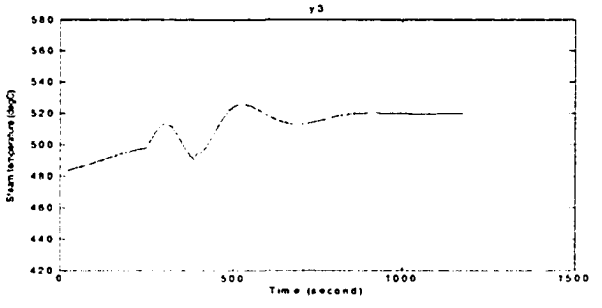

Figure 4-12: y_3 time response

Chapter 5

Conclusion

In this thesis, an input-output approach is used to control complex, industrial cogeneration systems. The design procedure is based on a multiple linear model representation, in which a set of linear models are identified for different operating points. The multiple robust H_∞ controllers based on multiple linear models are designed considering the linear model uncertainty and disturbance which goes into the system, and a supervisor is devised according to the input-output approach which is a novel controller design method by dealing with the stability issue. Simulation results demonstrate that the multiple robust controller reach good performance across the entire operating space.

The advantage of the multiple controller design method based on input-output approach is that linear controller design technique is applied. Linear controller design technique has sound theory basis, and it is simpler to design a linear controller than to design a nonlinear controller. Moreover, it is also relatively trivial to obtain multiple linear models than to obtain a nonlinear model for a complex nonlinear plant. Therefore, the multiple controller design approach based on the input-output approach is effective and practical for nonlinear control problem.

There still exist some open issues for future research work. In this thesis, three operating points are chosen according to the field operation experience. How to choose

appropriate operating points can be further studied. In addition, three local models are used to represent the original nonlinear plant. Therefore, the quantity of the local models should be studied theoretically. Finally, the model uncertainty is unknown in this thesis. If the exact model uncertainty information is known the controller would be less conservative. Thus, how to measure the uncertainty need be studied in the future.

Bibliography

[1] Wilson J. Rugh and Jeff S. Shamma (2000). Research on gain scheduling. Automatica36, 1401-1425

[2] Murry Smith, R. and T.A. Johansen (1997). Multiple model approaches to modelling and control. Taylor and Francis.

[3] H.J. Marquez (2000). An input-output approach to systems described using multiple models. IEEE Trans. Circuits and Systems6, 940-943

[4] D. Dougherty and D. Cooper (2003). A practical multiple model adaptive strategy for multivariable model predictive control. Control Engineering Practice 11, 649-664

[5] S.Gendron, M. Perrier, J.Barrette, M. Amjad, A. Holko and N. Legault (1993). Deterministic adaptive control of SISO processes using model weighting adaption. Int. J. Control 5, 1105-1123

[6] B.A. Foss, T.A. johansen and A.V. Sorensen (1995). Nonlinear predictive control using local models applied to a batch fermentation process. Control Engineering Practice 3, 389-396

[7] J.O. Trierweiler and A. R. Secchi (2000). Exploring the Potentiality of Using Multiple Model Approach in Nonlinear Model Predictive Control. Progress in Systems and Control theory, 26, 191-203

[8] A.S. Morse (1995). Control using logic-based switchng. Trends in Control: A European Perspective; Springer Verlag: London, 69-113

[9] Hideaki Ishii and Bruce A. Francis (2002). Stabilizing a linear system by switching control with dwell time. IEEE Tans. Auto. Contr.47(12), 1962-1973

[10] K.S. Narendra, J. Balakrishnan and M.K. Ciliz (1995). Adaptation and Learning Using Multiple Models, Switching, and Tuning. IEEE Contr. Syst. Mag., 37-51

[11] K.S. Narendra and J. Balakrishnan. (1997). Adaptive Control Using Multiple Models. IEEE Trans. Auto. Contr. 2, 171-187

[12] J.A. Rodriguez, J.A. Romangnoli and G.C. Goodwin (2003). Supervisory multiple regime control. Journal of Process Control 13, 177-191

[13] Peter Dorato (1987). A historical review of robust control. IEEE Control Systems Magazine, 44-47.

[14] Sam G. Dukelow (1991) The control of boilers (2nd Edition). Instrument society of America

[15] Ricky Leung (1997). Dynamic Simulation of An Utility Boiler's Natural-Circulation Circuit. University of Alberta, Master Thesis.

[16] Albert Chiu (1997). Dynamic Modelling and Simulation of an Industrial Boiler System. University of Alberta, Master Thesis.

[17] White David Michael (1996). Robust Controller Synthesis Utilizing Kharitonov's Theorem. University of Alberta, Master Thesis.

[18] Wen Tan, Horacio J. Marquez and Tongwen Chen (2002). Multivariable Robust Controller Design for a Boiler System. IEEE Trans. Control System Technoloty 10(5), 735-742

[19] Gordon Pellegrinetti and Joseph Bentsman (1994). H_∞ Controller Design for Boilers. International Journal of Robust and Nonlinear Control 4, 645-671

[20] Sigurd Skogestad and Ian Postlethwaite (1996). Multivariable Feedback Control Analysis and Design. John Wiley & Sons.

[21] R.W. Beaven, M.T. Wright and D.R. Seaward (1996). Weighting Function Selection in the H_∞ Design Process. Control Eng. Practice, 4(5), 625-633

[22] Chi-Tsong Chen (1999). Linear System Theory and Design. Oxford University Press.

[23] Kemin Zhou and John C. Doyle (1997). Essentials of Robust Control. Prentice Hall.

[24] R.H. Nyström, K.V. Sandström, T.K. Gustafsson and H.T. Toivonen (1999). Multimodel robust control of nonlinear plants: a case study. Journal of Process control, 9, 135-150.

[25] A. Banerjee and Y. Arkun (1995) H_∞ control of nonlinear processes using multiple linear models Proceedings of 3rd European control conference,Rome, Italy.

[26] L. Ljung (1987) System identification: Theory for the user. Prentice-Hall, Englewood cliffs, NJ.

[27] R.Gundala, K.A. Hoo and M.J. Piovoso (2000) Multiple Model Adaptive Control Design for a Multiple-Input Multiple-Output Chemical Reactor. Ind. Eng. Chem. Res. 39, 1554-1564.

[28] S. T. Clausen, P. Andersen and J. Stoustrup (2001). Robust Control. Lecture Notes.

[29] Z. Tian and K.A. Hoo. (2002). Transition Control Using Multiple Adaptive Models and an H-infinity Controller Design. 2002 American Control Conference.

[30] J.M. Maciejowski (1989). Multivariable feedback design. Addison-Wesley Publishing Company.

[31] T. Soderstrom and Pl Stoica (1989). System Identification. Prentice Hall.

[32] Young-Moon Park, Myoen-Song Choi, Jeong-Woo Lee and Kwang Y. Lee (1996). An Auxiliary LQG/LTR Robust Controller Design for Cogeneration Plants. IEEE Trans. Energy Conversion, 11(2), 407-413.

[33] Pang-Chia Chen and Jeff S. Shamma (2004). Gain-scheduled l^1-optimal control for boiler-turbine dynamics with actuator saturation. Journal of Process Control, 14, 263-277.

[34] K.J. Åström and R.D. Bell (2000). Drum-boiler Dynamics. Automatica, 36, 363-378.

[35] Hideaki Ishii and Bruce A. Francis (2002). Stabilizing a Linear System by Switching Control With Dwell Time. IEEE Tans. Auto. Contr.47(12), 1962-1973.

[36] Laurent Dubois, Francois Delmotte, Pierre Borne and Toshio Fukuda (1998). Stability Analysis of a Multiple-model Controller for Contrained Uncertain Nonlinear Systems. INT. J. Control, 69, 519-538.

[37] João P. Hespanha and A. Stephen Morse (2002). Switching Between Stabilizing Controllers. Automatica 38, 1905-1917.

[38] Andy Packard and Michael Kantner (1996). Gain Scheduling the LPV Way. Proceedings of the 35th Conference on Decision and Control, Kobe, Japan.3938-3941.

[39] T.A. Johansen, K.J. Hunt, P.J. Gawthrop and H.Fritz (1998). Off-equilibrium Linearisation and Design of Gain-schduled Control with Application to Vehicle Speed Control. Control Engineering Practice, 6, 167-180.

[40] Michael S. Branicky (1998). Multiple Lyapunov Functions and Other Analysis Tools for Switched and Hybrid Systems. IEEE Tans. Auto. Contr. 43(4), 475-482.

[41] A. Banerjee, Y. Arkun, B. Ogunnaike and R. Pearson (1997). Estimatio of Nonliear Systems Using Linear Multiple Models. Process Systems Engineering, 43(5), 1204-1226

[42] Philippos Peleties and Raymond DeCarlo (1992). Asymptotic Stability of m-switched Systems Using Lyapunov Functions. Proceedings of the 31st Conference on Decision and Control, Tusson, Arizona. 3438-3439.

[43] Adel Ben-Abdennour and Kwang Y. Lee (1996). An Automous Control System for Boiler-turbine Units. IEEE Trans. Energy Conversion, 11(2), 401-406.

[44] Z.G. Li, C.Y. Wen and Y.C. Soh (2001). Stabilization of a Class of Switched Systems via Designing Switching Laws. IEEE Tans. Auto. Contr.46(4), 665-670.

[45] Daniel Liberzon, João P. Hespanha and A. Stephen Morse (1999). Stability of Switched Systems: a Lie-algebraic Condition. Systems & Control Letters, 37, 117-122

[46] Kumpati S. Narendra and Jeyendran Balakrishnan (1994). A Common Lyapunov Function for Stable LTI Systems with Commuting A-Matrices. IEEE Tans. Auto. Contr.39(12), 2469-2471.

[47] Jovan D. Bošković (1997). A Multiple Model-Based Controller for Nonlinealy-Parametrized Plants. Proceedings of the American Control conference, Albuquerque, New Mexico, 2140-2144.

[48] Omar Galán, José A. Romagnoli and Ahmet Palazoglu (2000). Robust H_∞ Control of Nonlinear Plants Based on Multi-linear Models: An Application to a Bench-scale pH Neutralization Reactor. Chemical Engineering Science, 55, 4435-4450.

[49] Zhong Zhao, Xiaohua Xia, Jingchun Wang, Jian Gu and Yihui Jin (2003). Nonlinear Dynamic Matrix Control Based on Multiple Operating Models. Journal of Process Control, 13, 41-56.

[50] G.Davrazos and N.T. Koussoulas (2001). A Review of Stability Results for Switched and Hybrid Systems. 9th Mediterranean Conference on Control and Automation, Dubrovnik, Croatia.

[51] Daniel Liberzon and A. Stephen Morse (1999) Benchmark Problems in Stability and Design of Switched Systems. IEEE Control Systems Magazine, 59 - 70

[52] Philippos Peleties and Raymond DeCarlo (1992) Asymptotic Stability of m-Switched Systems Using Lyapunov-like Functions. Proceedings IEEE Conference on Decision and Control, 1679-1684.

[53] G.C. Goodwin, S.F. Graebe and M.E. Salgado (2001). Control system design. Prentice Hall.

[54] S.F. Graebe and Anders L.B. Ahlen (1996). Dynamic transfer among alternative controllers and its ralation to antiwindup controller design. IEEE Trans. Control System Technology 4 (1), 92-99

[55] Omar Galan, Jose A. Romagnoli and Ahmet Palazoglu (2000). Robust H_∞ control of nonlinear plants based on multi-linear models: an application to a bench-scale PH neutralization reactor. Chemical Engineering Sceience 55, 4435-4450

Appendix

The final low load controller is as follows,

$$\begin{aligned} \dot{x} &= A_l x + B_l y \\ u &= C_l x + D_l y \end{aligned}$$

Columns 1 through 3,

$$A_l = \begin{bmatrix} -0.00000014996383 & -0.00000018946012 & 0.00000014807409 \\ 0.00000001531488 & -0.00000089282510 & 0.00000136495302 \\ -0.00000011321067 & -0.00000073658838 & -0.00000534702122 \\ -0.00000020840194 & -0.00000141308077 & -0.00000781870518 \\ -0.00000007015347 & -0.00000464411291 & 0.00000801229136 \\ -0.00000001528755 & -0.00000495948826 & 0.00000303442698 \\ -0.00000001272394 & 0.00000171165661 & -0.00000991008536 \\ 0.00000006113807 & 0.00000180612245 & -0.00000789500087 \\ -0.00000001422905 & -0.00000023684939 & -0.00000016074025 \\ 0.00000001311651 & 0.00000155390883 & 0.00001456789230 \\ 0.00000001338701 & 0.00000076202425 & 0.00000732387473 \\ 0.00000005507344 & -0.00000165978015 & -0.00000323364896 \\ -0.00000000128684 & -0.00000016836682 & -0.00000001674884 \end{bmatrix}$$

Columns 4 through 7,

0.00000025033491	−0.00000067398867	−0.00000042398121	0.00000036185185
0.00000241258374	−0.00000660431379	−0.00000448998581	0.00000322278841
−0.00000975907477	0.00003292053958	0.00001430790124	−0.00002445980135
−0.00001895946942	0.00009988274827	0.00006028400463	−0.00005564813800
−0.00003468692969	−0.01922630602057	−0.02364507543551	0.01322227741220
−0.00003400325370	−0.02640324308084	−0.05327734533473	0.00640192946158
0.00000424964021	0.01709880598404	0.05292190794712	−0.03834478546172
0.00001347187964	0.01946904437949	0.06528419604292	−0.06598720232875
−0.00000314560542	−0.00183356515702	−0.00592950375568	0.00367448168949
0.00002145593198	−0.00406231120666	−0.00440850243416	0.04660932824940
0.00001132117844	−0.00181908716392	−0.00179949266721	0.02109174759776
−0.00000815181422	−0.00433347177277	−0.02027381268515	0.00869660470365
−0.00000130184598	−0.00105447315090	−0.00349628501135	0.00429169501212

Columns 8 through 11,

0.00000037479987	−0.00000003334077	0.00000027028505	0.00000012891296
0.00000322380973	−0.00000028266170	0.00000238952510	0.00000111952129
−0.00002762212666	0.00000254740836	−0.00001793459219	−0.00000922799057
−0.00005845296639	0.00000522720155	−0.00004192778080	−0.00002004912478
0.01141309312015	−0.00102793069048	0.00954237185909	0.00486005342975
−0.00914724218785	0.00023737496672	0.01363019378529	0.00756554376149
−0.01803676789998	0.00523079436114	−0.06725490561845	−0.03315657812353
−0.04793020616481	0.00597799642856	−0.07799823702361	−0.03808756804309
0.00447326300906	−0.00063889758098	0.01216096525361	0.00574506560841
0.05375501008569	−0.00726048713730	−0.07780055059341	−0.02792188874992
0.02393996634500	−0.00295346008143	−0.05096492212153	−0.02101562378933
0.00524583163054	−0.00131528819988	0.09823248923077	0.05113653624953
0.00481524260936	−0.00080450496686	0.00837202720318	0.00522754061588

Column 12 and 13

$$\begin{bmatrix} -0.00000000846755 & 0.00000001671893 \\ 0.00000015205726 & 0.00000015623147 \\ 0.00000591882903 & -0.00000086962361 \\ 0.00000263698291 & -0.00000255732556 \\ 0.00188405852858 & 0.00057523768983 \\ 0.01465074701767 & 0.00108091352925 \\ 0.01187547055595 & -0.00333680073676 \\ 0.02031413051265 & -0.00379438126533 \\ -0.00298024399215 & 0.00062038840487 \\ -0.04492768431682 & -0.01438513466572 \\ -0.01776924124016 & -0.00764488212697 \\ -0.04361683288681 & 0.00810318836938 \\ -0.01299103150770 & -0.00073416356187 \end{bmatrix}$$

$$B_l = \begin{bmatrix} -0.02548084282316 & -0.23844407701936 & -0.02537928355421 \\ -0.11476211357351 & 0.02474215116956 & -0.09807889909486 \\ 0.00750173376378 & -0.08068603293334 & -0.10473626529491 \\ -0.07493552154693 & -0.14835895928804 & -0.11244129157423 \\ -0.60508705664758 & -0.00160271401112 & 0.08639412722330 \\ -0.53330276186082 & 0.04741279983417 & -0.02684622887564 \\ 0.28563816005485 & -0.02886718900382 & -0.11275024078637 \\ 0.31796996227552 & 0.02886728910062 & -0.12339491833767 \\ -0.03048761167945 & -0.00851126286387 & 0.00187567410743 \\ -0.02594847362222 & -0.01158370019498 & 0.23508663287679 \\ -0.01042808643707 & -0.00013395991336 & 0.11399552591661 \\ -0.08419585097693 & 0.06514795948219 & -0.10683187575768 \\ -0.01706591416992 & 0.00101917599839 & -0.00227140321585 \end{bmatrix}$$

Columns 1 through 3,

$$C_l = \begin{bmatrix} -0.02709357688341 & -0.03284525132295 & -0.02193153338310 \\ -0.02937283099456 & -0.03220733284729 & -0.03259052966035 \\ -0.23780692618455 & -0.14589675932113 & 0.12646368019247 \end{bmatrix}$$

Columns 4 through 7,

0.01256221593767	−0.34185602854261	−0.44668084328730	0.00474655586925
0.01928106423398	−0.06234460010700	−0.08318981554171	−0.06194874816601
0.19934690500271	−0.50283642133390	−0.28449289662764	0.30211738229692

Columns 8 through 11,

−0.06657304452950	0.00785694441486	−0.06873468274062	−0.02175332732977
−0.08800568574435	0.00941941500692	0.01992568213814	−0.02174168018295
0.32401782694758	−0.02924033618490	0.22572492314922	0.11026257277021

Column 12 and 13,

$$\begin{bmatrix} 0.07244656900601 & -0.00520436434834 \\ 0.12858573569608 & 0.01009853463917 \\ -0.03103950449050 & 0.01297603978801 \end{bmatrix}$$

$$D_l = \begin{bmatrix} 0 & 0 & 0 \\ 0 & 0 & 0 \\ 0 & 0 & 0 \end{bmatrix}$$

The final normal load controller is as follows,

$$\begin{aligned} \dot{x} &= A_n x + B_n y \\ u &= C_n x + D_n y \end{aligned}$$

where,

Columns 1 through 3,

$$A_n = \begin{bmatrix} -0.00000082796509 & 0.00000019223261 & 0.00000025187467 \\ 0.00000002305564 & -0.00000195644186 & 0.00000019494566 \\ 0.00000020562997 & -0.00000013829428 & -0.00000112574713 \\ -0.00000205308733 & 0.00000142263361 & 0.00000659759021 \\ -0.00000065519188 & 0.00000133908390 & -0.00003965898214 \\ 0.00000011707920 & 0.00000032799601 & 0.00001098277349 \\ -0.00000268584228 & -0.00000300648277 & -0.00000768506482 \end{bmatrix}$$

Columns 4 through 7,

$$\begin{bmatrix} -0.00000089488767 & 0.00000231366608 & -0.00000016032436 & -0.00000032205069 \\ -0.00000233752997 & 0.00000407620701 & 0.00000039682288 & -0.00000758471765 \\ 0.00000915989491 & -0.00004082779445 & 0.00000627193084 & 0.00000142473903 \\ -0.00009349601337 & 0.00070734424823 & -0.00014394534888 & 0.00008987997834 \\ -0.00004983411686 & -0.03953024007920 & 0.01055090610079 & -0.00741791373166 \\ -0.00000037704323 & 0.01369814388528 & -0.00424413163498 & 0.00601489548374 \\ -0.00018750192082 & -0.03336075178739 & 0.01095819020849 & -0.02591878574999 \end{bmatrix}$$

$$B_n = \begin{bmatrix} -0.00846660464906 & 0.10509251114117 & 0.01636720982982 \\ -0.00093976955902 & 0.00959855644161 & -0.10547179317994 \\ -0.01221624800324 & -0.01410799443815 & -0.00463044542051 \\ -0.00230533387671 & 0.12747437227729 & 0.04808853776673 \\ -0.55218560592308 & -0.00805557994220 & 0.04073366720759 \\ 0.14284499404354 & 0.00262418052469 & 0.00789017576617 \\ -0.26817499393776 & 0.16414726805021 & -0.06453242999338 \end{bmatrix}$$

Columns 1 through 4,

$$C_n = \begin{bmatrix} 0.01677350887146 & -0.00435319842725 & -0.00905750491343 & 0.10730017838554 \\ 0.10471302162751 & -0.02410728132231 & -0.01440368774279 & 0.03494774540132 \\ 0.01174041524259 & 0.10303981395744 & -0.00895592714415 & 0.07637319177479 \end{bmatrix}$$

Columns 6 through 7,

$$\begin{bmatrix} -0.53132944777841 & 0.14242154725650 & -0.24055188310855 \\ -0.05020801925265 & -0.01142701194760 & 0.03624975441654 \\ -0.14765243009198 & -0.00770453307947 & 0.20939755090555 \end{bmatrix}$$

$$D_n = \begin{bmatrix} 0 & 0 & 0 \\ 0 & 0 & 0 \\ 0 & 0 & 0 \end{bmatrix}$$

The final high load controller is as follows,

$$\dot{x} = A_h x + B_h y$$
$$u = C_h x + D_h y$$

where,

Columns 1 through 3,

$$A_h = \begin{bmatrix} -0.00000099757874 & -0.00000010759244 & 0.00000167514689 \\ 0.00000000106170 & -0.00000104456414 & 0.00000068283696 \\ -0.00000007517771 & 0.00000386136394 & -0.00006133793902 \\ -0.00000000298295 & 0.00000000080541 & 0.00000005497079 \\ -0.00000146342469 & -0.00000218762175 & 0.00007597064611 \\ -0.00000084526851 & -0.00000378787547 & 0.00010469751550 \\ 0.00000085030588 & 0.00000200997385 & -0.00006649654725 \\ -0.00000003757018 & -0.00000002919701 & 0.00000091765103 \\ -0.00000013312759 & -0.00000031148351 & 0.00000882095509 \end{bmatrix}$$

Columns 4 through 7,

−0.00000004151852	−0.00000636858176	0.00000220665782	0.00000167843264
−0.00000002697453	−0.00000369121582	0.00000234013599	−0.00000082274338
0.00000394417227	0.00047395872629	−0.00020101751891	−0.00008823861713
−0.00000211595162	−0.00014215498911	0.00017079718848	−0.00002250045433
−0.00029036002522	−0.03230038176074	0.02383682284173	0.00701945538616
0.00013844420605	0.01691552636675	−0.03150213661559	0.02613119503446
0.00010392936434	0.01829860335813	−0.03547004962974	−0.01690008798981
−0.00000219574687	−0.00044403526307	0.00065904745816	0.00097744947090
0.00000576725596	0.00042065606575	−0.00377603197804	0.00274653377597

Column 8 and 9,

$$\begin{bmatrix} -0.00000000252927 & 0.00000018293632 \\ -0.00000006382490 & -0.00000001466837 \\ -0.00000032962887 & -0.00001035633940 \\ 0.00000201422873 & -0.00000036271023 \\ 0.00013214690665 & 0.00123082811416 \\ -0.00078137059665 & 0.00103864373545 \\ -0.00032291348510 & -0.00478176467972 \\ -0.00001512511507 & 0.00019852082626 \\ -0.00018529023435 & -0.00032195906730 \end{bmatrix}$$

$$B_h = \begin{bmatrix} -0.00496814608083 & 0.04325491733081 & -0.25491374167570 \\ -0.00620276667369 & 0.11857619115514 & 0.01747094538674 \\ -0.00157676283960 & -0.22041636481894 & -0.04454697847839 \\ 0.00991909070709 & 0.00055043373608 & -0.00049596491392 \\ 0.83465743428830 & 0.19709777313313 & -0.17554983844288 \\ -0.39780603192946 & 0.20937165710735 & -0.06783874625302 \\ -0.22706682159587 & -0.14230430438797 & 0.09210393037215 \\ 0.00447978422657 & 0.00260842976878 & -0.00458494942412 \\ -0.01531804563268 & 0.01936149393283 & -0.01392063213900 \end{bmatrix}$$

Columns 1 through 3,

$$C_h = \begin{bmatrix} -0.00071936363776 & 0.02338397506814 & -0.05595250641324 \\ -0.00365790063135 & 0.11667379932889 & -0.01365150501161 \\ 0.25857839879391 & 0.01563443686880 & -0.21737811939040 \end{bmatrix}$$

Columns 4 through 7,

$$\begin{bmatrix} 0.00831901245445 & 0.28208542300798 & -0.35101738683920 & 0.17794752636623 \\ -0.00079626175878 & 0.05097929138650 & -0.02931465438481 & 0.04192450123070 \\ 0.00539419298390 & 0.82713193417993 & -0.28742941830547 & -0.21649481417276 \end{bmatrix}$$

Column 8 and 9,

$$\begin{bmatrix} -0.00503695706566 & 0.01558191966156 \\ 0.00473054244113 & 0.00091726577151 \\ 0.00038100595121 & -0.02365705754375 \end{bmatrix}$$

$$D_h = \begin{bmatrix} 0 & 0 & 0 \\ 0 & 0 & 0 \\ 0 & 0 & 0 \end{bmatrix}$$